JOURNAL OF PROPULSION AND POWER
Vol. 33, No. 3, May–June 2017

Recommended Practice for Thrust Measurement in Electric Propulsion Testing

James E. Polk*
Jet Propulsion Laboratory, California Institute of Technology, Pasadena, California 91109
Anthony Pancotti†
MSNW, LLC, Redmond, Washington 98052
Thomas Haag‡
NASA John H. Glenn Research Center, Cleveland, Ohio 44135
Scott King§ and Mitchell Walker¶
Georgia Institute of Technology, Atlanta, Georgia 30332
Joseph Blakely**
ERC, Inc., Edwards Air Force Base, California 93523
and
John Ziemer††
Jet Propulsion Laboratory, California Institute of Technology, Pasadena, California 91109

DOI: 10.2514/1.B35564

The accurate, direct measurement of thrust or impulse is one of the most critical elements of electric thruster characterization, and it is one of the most difficult measurements to make. This paper summarizes recommended practices for the design, calibration, and operation of pendulum thrust stands, which are widely recognized as the best approach for measuring micronewton- to millinewton-level thrust and micronewton-per-second-level impulse bits. The fundamentals of pendulum thrust stand operation are reviewed, along with the implementation of hanging pendulum, inverted pendulum, and torsional balance configurations. The methods of calibration and recommendations for calibration processes are presented. Sources of error are identified, and methods for data processing and uncertainty analysis are discussed. This review is intended to be the first step toward a recommended practices document to help the community produce high-quality thrust measurements.

Nomenclature

A_F	=	amplitude of thrust stand response due to impulse, V
A_N	=	noise amplitude, V
b	=	estimate of β from calibration fit, V
c	=	damping constant, N · ms/rad
d_1, d_2	=	constants associated with damped motion
e_i	=	differences between predicted and measured responses to calibration loads, V
F	=	applied force, N
F_{cal}	=	calibration force, N
F_i	=	calibration forces, N
F_t	=	thrust force, N
$\bar{F}$	=	mean of calibration forces, N
$\bar{F}_t$	=	amplitude of a periodic forcing function, N
G	=	sensor responsivity, V/m
g	=	acceleration due to gravity, m/s^2
I	=	moment of inertia, kg · m^2
I_{bit}	=	impulse bit, N · s
k	=	effective spring constant associated with restoring forces, (N · m)/rad
k_s	=	spring constant, (N · m)/rad
L	=	distance between pendulum pivot and point where force is applied, m
L_{cal}	=	distance between pendulum pivot and point where calibration force is applied, m
L_{cm}	=	distance from center of mass to pendulum pivot, m
L_{pm}	=	distance between point of deflection measurement and pendulum pivot, m
L_t	=	distance between pendulum pivot and point where thrust force is applied, m
M_t	=	thruster mass, kg
m	=	mass, kg
N	=	number of repeat thrust measurements at a given operating point
n_i	=	number of calibration measurements
R	=	correlation coefficient
$\mathcal{S}$	=	thrust stand sensitivity, m/N or V/N
S_{cal}	=	estimate of the thrust stand sensitivity $\mathcal{S}$ from calibration fit, m/N or V/N
s_{F_t}	=	estimate of standard deviation of thrust measurement σ_{F_t}, N
s_{Scal}	=	estimate of standard deviation of thrust stand sensitivity, V/N
s_x^2	=	estimate of variance σ_x^2, V^2
$\mathcal{T}_g$	=	torque due to gravity, N · m
t	=	time, s
u_i	=	disturbances (errors) in calibration measurements, V
V_{ss}	=	sensor output corresponding to linear displacement, V
W	=	thruster weight, N
x	=	linear displacement, m
x_{FS}	=	full-scale deflection, m
x_i	=	measured responses to calibration forces, V
x_{ss}	=	steady-state linear displacement, M

Received 16 August 2014; revision received 30 June 2016; accepted for publication 30 June 2016; published online 21 April 2017.

*Principal Engineer, Propulsion, Thermal and Materials Engineering Section, M/S 125-109, 4800 Oak Grove Drive. Associate Fellow.
†Advanced Propulsion Research Scientist.
‡Aerospace Engineer, Space Propulsion Branch.
§Graduate Research Assistant, School of Aerospace Engineering.
¶Associate Professor, School of Aerospace Engineering.
**Electric Propulsion Research Scientist.
††Concept Innovation Methods Chief, JPL Innovation Foundry.

$\bar{x}$ = mean of measured responses to calibration loads, V
$\hat{x}_i$ = predicted responses to calibration loads, V
$\bar{x}_t$ = mean of N repeat thrust measurements at a given operating point, N
β = intercept of calibration line, V
Δx_{ss} = displacement of thrust stand, m
$\Delta\dot{x}$ = change in linear velocity due to impulse, m/s
$\Delta\dot{\theta}$ = change in angular velocity due to impulse, rad/s
$\delta(t)$ = Dirac delta function
ζ = damping coefficient
θ = angular deflection, rad
θ_m = maximum amplitude of oscillations, rad
θ_{ss} = steady-state angular deflection under load, rad
θ_{st} = steady-state deflection due to a static load, rad
θ_z = thrust stand tilt from the vertical axis, rad
σ_{F_t} = standard deviation of thrust measurement, V
σ_x^2 = variance of thrust stand response to calibration loads, V^2
τ = impulse duration, s
τ_n = natural period, s
Ω = ratio of the frequency of a periodic load to the natural frequency
ω = frequency of a periodic load, s^{-1}
ω_d = frequency of damped motion, s^{-1}
ω_n = natural frequency, s^{-1}

I. Introduction

AS PART of a larger effort by the American Institute of Aeronautics and Astronautics' (AIAA's) Electric Propulsion Technical Committee to provide standards for electric thruster measurement and test, we have developed recommendations for direct thrust measurements. Measurement of thrust is one of the most fundamental requirements in thruster performance characterization. Because electric thrusters produce relatively low-thrust levels, direct thrust measurements can be challenging. Thrust measurements are particularly difficult for microthrusters, which have enjoyed increased attention in the last two decades. Considerable effort and talent have been invested in developing sensitive thrust stands and measurement techniques, and one objective of the AIAA initiative is to capture this knowledge and distill it for the community.

The purpose of this paper is to recommend best practices for the use of the most common types of pendulum thrust stands based on experience from the community; it is not to specify a particular thrust stand design that must be used to produce credible results. These recommendations include best practices for the design, calibration, and operation of pendulum thrust stands and the analysis of thrust stand data with a particular focus on cataloguing sources of error and estimating the uncertainty in the measurements. The goals are to help users avoid common mistakes, improve the quality of thrust stand measurements with proven approaches to thrust stand use, and provide guidelines for reporting results to make it easier to evaluate the reliability of thrust stand measurements.

This paper provides an overview of the three types of pendulum thrust stands (inverted, hanging, and torsional), including the dynamics that underlie their operation and key performance metrics. Typical implementations and how they are optimized are then described. Methods for calibration, operation, and data analysis are discussed along with typical sources of error, methods to control errors, and the process of estimating measurement uncertainties. Finally, we provide a list of items that should be included when reporting thrust measurements.

II. Thrust Stands for Electric Propulsion

A. Overview

High-thrust devices are often tested on load cells. However, because most electric thrusters have low-thrust-to-weight ratios, a load cell signal would be dominated by the weight of the thruster. To address this issue, the thrust or impulse bit from electric thrusters is typically inferred from the motion of pendulum thrust stands. Three major configurations (hanging pendulums, inverted pendulums, and torsional pendulums) are used to make accurate steady-state and impulse thrust measurements. All of these configurations are variations of a spring–mass–damper system, as illustrated in Fig. 1. Although each of these implementations has its advantages and disadvantages, pendulum thrust stands in general are widely accepted as a reliable way to make direct thrust measurements with electric thrusters.

B. Pendulum Thrust Stand Dynamics.

Many characteristics of pendulum thrust stands can be understood by examining three solutions to the equation of motion for ideal pendulums. The equation of motion for a second-order system relates the time rate of change of angular momentum to the sum of torques due to torsional springs, dampers, and applied forces [1]. The dynamics of all three types of pendulums are described by the same equation:

$$I\ddot{\theta} + c\dot{\theta} + k\theta = F(t)L \tag{1}$$

where θ is the angular position relative to a reference position, I is the moment of inertia, c is the damping constant, k is the effective spring constant associated with restoring forces, and $F(t)$ is an applied force acting at a distance L from the pivot that produces a torque on the system. I, c, and k are assumed to be constants. Actual thrust stands may include active components, such as electronic dampers where the damping constant is frequency dependent, which complicates the analysis. This equation can be cast in the standard form

$$\ddot{\theta} + 2\zeta\omega_n\dot{\theta} + \omega_n^2\theta = F(t)L/I \tag{2}$$

where ζ is the damping coefficient,

$$\zeta = \frac{c}{2}\sqrt{\frac{1}{Ik}} \tag{3}$$

and ω_n is the natural frequency of the undamped system:

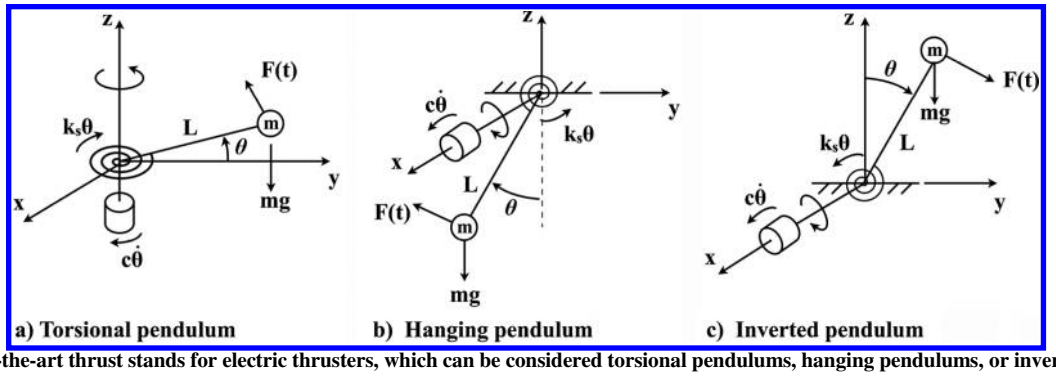

Fig. 1 State-of-the-art thrust stands for electric thrusters, which can be considered torsional pendulums, hanging pendulums, or inverted pendulums.

$$\omega_n = \sqrt{\frac{k}{I}} \tag{4}$$

The primary difference in the three types of pendulum thrust stands is the effect of the gravity force on the dynamics. Gravity acts as a restoring force in hanging pendulums (a force tending to increase the deflection in inverted pendulums) and has no influence on ideal torsional pendulums where the plane of motion is perpendicular to the gravity vector. The torque associated with the gravitational force in hanging and inverted pendulums is

$$\mathcal{T}_g = mgL_{\text{cm}} \sin\theta \simeq mgL_{\text{cm}}\theta \tag{5}$$

where m is the mass, g is the acceleration due to gravity, and L_{cm} is the distance from the center of mass to the pivot point. The second expression is valid for small deflection angles. For example, the error in the gravitational torque associated with this approximation is less than 0.13% for angles of 5 deg or less. In this approximation, where the gravity torque is proportional to the deflection, it can be incorporated in the spring torque term of Eq. (1):

$$k = \begin{cases} k_s + mgL_{\text{cm}} & \text{for hanging pendulums} \\ k_s - mgL_{\text{cm}} & \text{for inverted pendulums} \end{cases} \tag{6}$$

Clearly, for inverted pendulums, the gravity torque must not exceed the spring torque; otherwise, the restoring force is negative and the pendulum is unstable.

Equation (2) can be solved to give the response of a pendulum to an arbitrary input force. Three special cases with analytical solutions are particularly relevant for pendulum thrust stands. The dynamic motion of a pendulum thrust stand subject to the torque produced by a constant thrust F_t from a steady-state thruster applied at a distance L_t from the pivot can be approximated by the response of an ideal pendulum to a step input with initial conditions $\theta(0) = \dot{\theta}(0) = 0$, where

$$F(t) = \begin{cases} 0 & \text{for } t < 0 \\ F_t & \text{for } t \geq 0 \end{cases} \tag{7}$$

The deflection $\theta(t)$ normalized by the steady-state deflection

$$\theta_{\text{ss}} = \frac{F_t L_t}{I\omega_n^2} = \frac{F_t L_t}{k} \tag{8}$$

depends on the damping coefficient:

$$\frac{\theta(t) I\omega_n^2}{F_t L_t} = \frac{\theta(t)}{\theta_{\text{SS}}} = \begin{cases} 1 - e^{-\zeta\omega_n t}\left[\cos(\omega_d t) + \frac{\zeta}{\sqrt{1-\zeta^2}}\sin(\omega_d t)\right] & \text{for } \zeta < 1 \text{(underdamped)} \\ 1 - e^{-\omega_n t}(1 - \omega_n t) & \text{for } \zeta = 1 \text{(criticallydamped)} \\ 1 + \frac{1}{2\sqrt{\zeta^2-1}}\left[\frac{1}{d_1}e^{-d_1\omega_n t} - \frac{1}{d_2}e^{-d_2\omega_n t}\right] & \text{for } \zeta > 1 \text{(underdamped)} \end{cases} \tag{9}$$

In these expressions, $\omega_d = \omega_n\sqrt{1-\zeta^2}$ is the frequency of the damped motion, $d_1 = \zeta - \sqrt{\zeta^2 - 1}$, and $d_2 = \zeta + \sqrt{\zeta^2 - 1}$. Example responses plotted in Fig. 2 show that the time required to reach the steady-state deflection depends on the damping coefficient. The settling time, defined as the time required to settle within 2% of the steady-state deflection, is about one period for critically damped pendulums and depends on the damping coefficient for overdamped and underdamped pendulums. This is a fundamental limit on the response time for step changes in thrust levels for pendulum thrust stands.

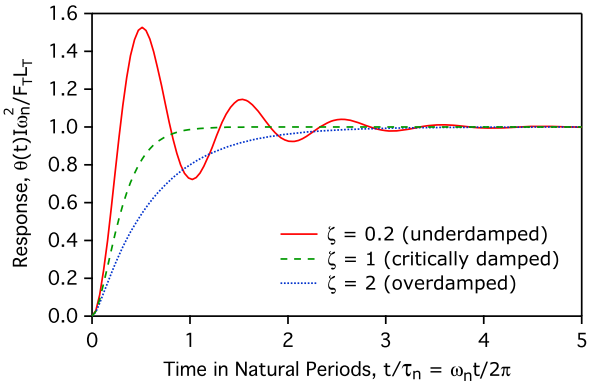

Fig. 2 Response of under-, over-, and critically damped pendulums to a step input, normalized by the steady-state deflection.

The response of a pendulum thrust stand to the impulse bit from a pulsed thruster applied at a distance L_t from the pivot may be approximated by the solution to Eq. (2) for an impulse input of $F(t) = I_{\text{bit}}\delta(t)$, where $\delta(t)$ is the Dirac delta function, with initial conditions $\theta(0) = \dot{\theta}(0) = 0$:

$$\frac{\theta(t) I\omega_n}{I_{\text{bit}} L_t} = \begin{cases} \frac{1}{\sqrt{1-\zeta^2}} e^{-\zeta\omega_n t}\sin(\omega_d t) & \text{if} \zeta < 1 \text{(underdamped)} \\ \omega_n t e^{-\omega_n t} & \text{if } \zeta = 1 \text{(criticallydamped)} \\ \frac{1}{2\sqrt{\zeta^2-1}}\left[e^{-d_1\omega_n t} - e^{-d_2\omega_n t}\right] & \text{if } \zeta > 1 \text{(underdamped)} \end{cases} \tag{10}$$

Example solutions plotted in Fig. 3 show that the response is a transient with a decay time determined by the damping coefficient. As the expanded plot in the upper right portion of this figure suggests, all three curves have the same initial slope, reflecting the fact that the initial angular velocity produced by the impulse is independent of the damping coefficient. The change in velocity due to the impulse is

$$\Delta\dot{\theta}(0) = I_{\text{bit}} L_t / I \tag{11}$$

It can also be shown that the maximum amplitude θ_m and the range (difference between the first peak and the first valley) of the response are proportional to the impulse bit. For example, for an undamped oscillator ($\zeta = 0$), the maximum amplitude is

$$\theta_m = I_{\text{bit}} L_t / I\omega_n \tag{12}$$

The peak amplitude and range decrease as the damping coefficient increases. The equations of motion can also be solved for finite pulse lengths [2] and for repeated impulses [3].

If the force on the thrust stand is time varying, the response also varies in time and the amplitude depends on the frequency of the applied force compared to the natural frequency of the stand. For a periodic forcing function of the form $F(t) = \bar{F}_t\cos(\omega t)$, the response will initially include a transient component at a frequency of

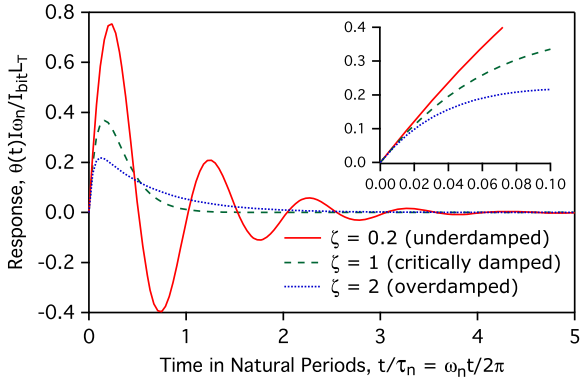

Fig. 3 Normalized response to an impulse input.

ω_d and a steady-state component at the driving frequency ω. After the transient response dies out, the amplitude of the steady-state oscillation compared to the deflection $\theta_{st} = \bar{F}_t L_t/k$ due to a static load of $\bar{F}_t$ is

$$\frac{\bar{\theta}}{\theta_{st}} = \frac{1}{[(1-\Omega^2)^2 + (2\zeta\Omega)^2]^{1/2}} \tag{13}$$

where $\Omega = \omega/\omega_n$. This function is plotted in Fig. 4 for a range of damping ratios. For critically damped (and overdamped) pendulums, the response amplitude decays monotonically with input frequency. As expected though, underdamped pendulums can have an amplified response when the driving frequency approaches the resonant frequency of the stand. For frequencies above the resonance, the response is attenuated. The sensitivity of a pendulum thrust stand to dynamic thrust loads therefore varies with frequency.

C. Thrust Stand Performance Metrics

The quality of thrust measurements depends on six thrust stand performance metrics, which we review in this section. Ways to characterize these parameters and achieve high-thrust stand performance are discussed in subsequent sections.

1. *Sensitivity*

The thrust stand sensitivity is one of the most important figures of merit because it largely determines the precision and resolution of thrust measurements. The sensitivity for a steady-state thrust measurement can be defined as the deflection achieved for a given applied force. As Eq. (8) shows, this depends on the length of the moment arm L_t and the effective spring constant k, and is therefore a key mechanical design feature of the stand.

In practice, the sensitivity depends on the ability to measure the deflection, and it is often expressed as the voltage output of a position transducer for a given force (in volts per newton). There are many ways to measure the angular deflection as a function of time $\theta(t)$. For small deflections where the small angle approximation is valid, the linear displacement $x(t) \simeq L_{pm}\theta(t)$ at a point a distance L_{pm} from the pivot can be measured. Often, the linear displacement can be measured more accurately than the angular deflection, but at the expense of the error introduced by the need to measure L_{pm}. In this case, the sensitivity is given by

$$x_{ss}/F_t = L_{pm}L_t/k = L_{pm}L_t/I\omega_n^2 \tag{14}$$

where x_{ss} is the steady-state position. This is typically reported as the position sensor output $V_{ss} = Gx_{ss}$, where G is the sensor responsivity in volts per meter. The responsivity is an important design parameter, and a very sensitive transducer may compensate for small deflections, which may be necessary to remain in the linear regime or because of other constraints.

For impulse measurements, the sensitivity may be defined as the initial velocity of the pendulum or the maximum deflection obtained for a given impulse; for example,

$$\Delta\dot{x}(0)/I_{bit} = L_{pm}L_t/I \tag{15}$$

This can be similarly translated into the response of a transducer to a given input.

As noted previously, the thrust stand sensitivity can vary with frequency for dynamic thrust loads. To achieve a flat response for relevant thrust input frequencies, the stand should be designed to be underdamped with a damping ratio of ~0.5–0.6 and a natural frequency much higher than the input frequencies. High natural frequencies can be achieved with high stiffness or a low moment of inertia. Of these strategies, decreasing the moment of inertia is preferred; otherwise, sensitivity (which scales inversely with stiffness) will be sacrificed for a flat response. The amplification in response near the resonant frequency has been exploited in at least one design [4] to increase sensitivity. In this approach, a pulsed thruster was fired every half-period at the natural frequency of a minimally damped torsional thrust stand in order to amplify the amplitude of the stand oscillation and achieve sub-micronewton sensitivity.

Although the sensitivity can be estimated from the design parameters in Eq. (14), a value determined by calibration with known forces or impulses should be used to accurately calculate the thrust or impulse bit associated with a measured deflection. If the sensitivity is calibrated directly by applying known forces or impulses at L_t, then the geometric parameters such as L_t and L_{pm} do not need to be known. Calibration of the thrust stand response is one of the most important steps in thrust measurement, and it is discussed in detail in Sec. IV.

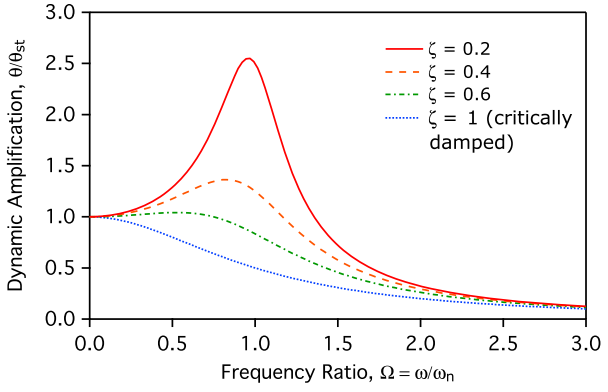

Fig. 4 Amplitude of pendulum response due to a periodic force $F(t) = \bar{F}_t \cos(\omega t)$, normalized by the deflection θ_{st} due to a static load $\bar{F}_t$.

2. *Repeatability and Long-Term Stability*

The use of a sensitivity calibration performed before and/or after a thrust measurement relies on the assumption that the thrust stand response is repeatable, so this has a first-order impact on measurement accuracy. The stability of thrust stand response is also important in long-duration time-resolved thrust measurements. Repeatability can be affected by two factors: 1) drifts that cause a shift in the apparent or real position of the pendulum (zero shifts) and 2) variability in the responsivity G or the effective spring constant k (gain shifts). These effects are often due to temperature changes in mechanical or electronic components or to parasitic spring or friction forces, and they must be carefully controlled in the design. Various methods to control or correct for drift and minimize parasitic forces are discussed in the following. The residual variability in the response must be characterized by repeated calibration measurements under different conditions to determine its contribution to the error estimate, which is discussed in Sec. VI.

3. *Accuracy*

Accuracy is a measure of the error between a thrust stand measurement and the true value of the thrust. In addition to being

precise (which is ensured if the thrust stand is sufficiently sensitive, repeatable, and not subject to large random errors), it must produce accurate results. High accuracy in a precise thrust measurement is achieved by minimizing systematic errors, and it can only be demonstrated by calibration measurements of known forces or impulses. To properly demonstrate that a thrust stand meets a given accuracy requirement, the calibration method must be carefully designed so that it reproduces the conditions of the actual thrust measurement and does not introduce additional systematic errors.

4. *Resolution*

Resolution is defined as the smallest difference between two thrust or impulse inputs that can be reliably distinguished in the thrust stand response. The resolution is ultimately limited by the noise level of the stand's response, so achieving high resolution depends on minimizing noise. Sources of noise typically include the electrical noise associated with sensors, mechanical noise due to vibrations in the environment that are transmitted to the thrust stand, and (on long timescales) variations in thrust stand response that may be caused by periodic changes in temperature, for instance. Thrust stand resolution can be quantified by varying the difference between two input loads until the responses become indistinguishable [5]. In practice, this approach may not be feasible, and resolution is often inferred from measured noise levels.

In some cases, the frequency-dependent thrust noise level generated by the thruster is an important measurement parameter. For instance, the thrusters for the Space Technology 7/Laser Interferometer Space Antenna (ST7/LISA) Pathfinder mission had to demonstrate a thrust noise level less than 0.1 $\mu\text{N}/\sqrt{\text{Hz}}$ for frequencies between 1 mHz and 4 Hz, which is a requirement driven by the control algorithm for the disturbance reduction system [6]. In addition to having adequate frequency response, as discussed previously, the thrust stand must have a noise floor (noise in the response with no thrust load) significantly lower than the requirement the thruster must meet. The noise floor can be characterized either by amplitude vs frequency or by the power spectral density. This may also be considered the frequency-dependent resolution of the thrust stand. Figure 5 shows an example noise spectrum for the thrust stand described in Sec. III.D.

5. *Response Time*

The thrust stand response time is an important metric for time-resolved measurements, and it can be characterized by a number of parameters. Quantitative metrics based on a step input include the rise time (time required to reach 100% of the steady-state value), the peak time (time required to reach the peak response), the maximum overshoot, and the settling time t_s (the time required for the variations around the steady-state value to drop to within 2% of that value). Figures 2 and 3 illustrate the effect of damping ratio on these parameters. A damping ratio of $0.4 \leq \zeta \leq 0.8$ generally gives a good step response. For this range, $t_s = 4/\zeta\omega_n$.

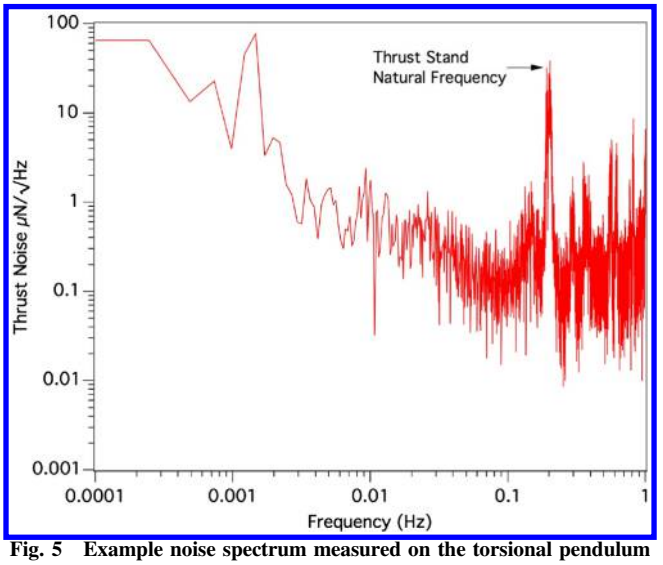

Fig. 5 Example noise spectrum measured on the torsional pendulum shown in Fig. 9. This noise floor defines the frequency-dependent resolution of the thrust stand.

6. *Predictability of the Response*

The response of an ideal pendulum is linear in the small angle approximation presented in Sec. II.B. A pendulum thrust stand need not have a linear response, depending on the characteristics of the spring, damper, and position sensor components, but it is good practice to design the stand so this is the case. At a minimum, the transfer function must be known so that sensitivity calibration data can be interpreted in terms of a physical model. Deviations from the known linear (or nonlinear) functional form measured in a calibration can be used to estimate the contribution of the calibration process to the overall error or to identify systematic problems that need to be resolved before proceeding with a thrust measurement.

Transfer function complexity often depends primarily on the behavior of damping elements in the thrust stand. Active electronic spring/damper systems can be designed to provide a force that is proportional to the deflection or the velocity of the pendulum, or to the integral of the deflection [proportional/integral/derivative (PID) control], which results in a much more complex transfer function compared to passive linear elements such as eddy current or viscous dampers. Active control can provide improved transient response, but at the price of greater complexity of the measurement system and analysis.

In addition to these quantitative performance metrics, other considerations such as ease of use and compatibility with calibration methods play a role in thrust stand design.

III. Thrust Stand Configurations and Components

All three basic pendulum configurations have been successfully employed with electric thrusters, and each has its own advantages and challenges. In this section, we review the unique features of each approach and discuss example designs that have provided excellent performance for their applications. First, however, we describe options for components that are common to all thrust stand configurations.

A. Components Common to All Pendulum Thrust Stands

All pendulum thrust stands require displacement sensors and spring elements, and most incorporate dampers. Displacement sensors are a key element in meeting performance requirements. They are typically noncontact devices to prevent hysteresis from mechanical drag and have a range and resolution chosen to match the thrust stand design deflection. Sensors that have been used successfully on thrust stands include linear variable differential transformers (LVDTs; also known as linear variable differential transducers) [2,7–10], capacitive sensors [11], optical interferometers [5,12,13], reflectance fiber optic sensors [14], autocollimators [15], laser triangulation systems [16], and photoelectric position sensors [17]. In this section, we review LVDTs and laser interferometers: two sensor options that bracket the measurement range and resolution required for electric propulsion thrust stands.

A recommended option for thrust stand designs with relatively large deflections (on the order of a millimeters) is the LVDT, which consists of two components. The transformer, which is typically mounted on the fixed part of the thrust stand, is a tube with three solenoidal windings spaced along the axis. The primary is in the center and two secondaries wound in opposite directions are located symmetrically on either side of the primary. A cylindrical ferromagnetic core attached to the pendulum moves freely along the fixed transformer axis. The primary is driven with an ac current, which induces a voltage in each secondary winding that depends on the location of the core. The difference between the two secondary winding signals is a sensitive measure of the core's position.

Commercial LVDTs typically have a response that is linear to within 0.25–0.5% of full scale (FS) within the specified range, which can be from less than 1 mm to as high as 500 mm. LVDTs are extremely stable, with a temperature sensitivity on the order of 0.02% FS per degree Celsius and a repeatability on the order of. 01% FS. The analog signal offers unlimited spatial resolution in principle. In practice, it is limited by electrical noise, but submicrometer resolution is achievable [8]. The sensors (particularly ac LVDTs, which do not have electronics integrated with the transformer housing) are relatively immune to electrical noise from thrusters.

Optical interferometers offer much higher sensitivity and resolution, and they have been used successfully on thrust stands with very small deflections [5,12,13], although they are a more expensive solution. In a basic interferometer, a coherent light beam is split into two beams using a beam splitter. The beams are directed along different paths and then recombined. If the path lengths are different by a noninteger multiple of the wavelength, the beams will have different phases and will interfere either constructively or destructively. The amplitude of the combined light signal will therefore vary periodically as the path length changes. By reflecting one beam from the movable pendulum and the other from the fixed base of the thrust stand and then recombining them, changes in the relative displacement can be calculated from the time-dependent periodic amplitude of the combined signal measured with one or more photodiodes. Cubbin [12] developed a Michelson interferometer [18], with a range of tens of micrometers and a resolution based on measured noise of 10 nm. The nanobalance described in Sec. III.C [5,13] employs a high-resolution Fabry–Pérot interferometer [18]. The measurement range is on the order of 150 nm (for a 1 mN full-scale thrust level), and the frequency resolution of the cavity corresponds to a spatial resolution of 14 pm. The phase [12] or frequency [13] measurement with interferometers is linearly related to the displacement. The photodiodes used in these systems proved to be immune to electrical noise from the thrusters.

To damp thrust stand oscillations, passive eddy current dampers [17,19–24] and active electromagnetic dampers [7,25,26] have primarily been employed, although oil dampers have also been used [9,10]. Eddy current dampers are simple, noncontact mechanisms consisting of two stationary magnets between which a conducting plate (typically copper) moves. The magnetic field induces eddy currents in the plate, which interact with the magnetic field to generate a Lorentz force proportional to velocity that opposes the motion. Active electromagnetic force actuators consist of a ferromagnetic core that moves along the axis of a solenoid. The force on the core is proportional to the current in the solenoid. A closed-loop PID controller is often used to vary the solenoid current to damp out time-dependent components of the thrust stand motion. Active dampers provide more flexibility in tuning and can be turned off to observe the free motion of the thrust stand (for impulse measurements, for example).

The spring elements of a thrust stand consist of the pendulum pivot; any springs deliberately added to increase or fine-tune the spring force; and wires or tubing that cross between moving and stationary parts of the thrust stand, producing parasitic spring forces. Pendulum pivots can consist of simple flat-plate flexures [25,26] or more complex flexural pivots [8,9,14,16,23], which are commercially available. Beams resting on knife edges are sometimes used as the pivot points for hanging pendulums to minimize the restoring force [27]. Some torsional thrust stand variants use thin beryllium [22] or tungsten [15,28] wire to support the weight of the beam. The wire diameters are typically on the order of 0.5 mm [15], and the torsion spring constant of the wire provides the restoring force. However, flexural pivots allow a higher beam system mass (including thruster and counterweights).

Electrical conductors, propellant and cooling water tubing, and instrumentation wiring that cross the interface between the facility and the movable pendulum also contribute to the effective spring constant. These components must be carefully chosen to provide repeatable behavior. Although finely stranded, braided conductors may minimize reaction forces imparted through the thrust stand, internal friction during flexure often results in nonrepeatable tares and unacceptable levels of uncertainty in thrust measurements. Similarly, soft polymer tubing often exhibits viscoelastic behavior that varies significantly with temperature. Solid metal tubing should be used to maximize linearity and repeatability. Novel approaches to minimizing the spring force from these elements include the use of liquid gallium pots to transfer electric power [19,20,29] and an oil seal in the gas feed line on the axis of a torsional pendulum [9,10]. The oil pot also serves as a viscous damper in this design.

B. Inverted Pendulum Thrust Stands

Inverted pendulum thrust stands have two main advantages: they can achieve high sensitivity and are very compact. In its simplest form, an inverted pendulum consists of a vertical arm attached to a bottom pivot or flexure with the thruster mounted at the top. With an inverted pendulum configuration, the torque produced by the thruster weight counters the spring torque and reduces the effective spring constant, as shown in Eq. (6). By carefully balancing the length of the pendulum and the thruster mass with the spring stiffness so that the gravity torque approaches the spring torque, very large deflections in proportion to applied thrust can be obtained. Deflections of several millimeters are commonly achieved with pendulum lengths less than 20 cm, permitting use in vacuum chambers less than 1 m in diameter [30].

However, these characteristics lead to several challenges. Inverted pendulum thrust stands are very sensitive to changes in the inclination of the stand with respect to the gravity vector. The thrust stand deflection when the z axis is parallel to the gravity vector, as shown in the idealized configuration in Fig. 1, is given by Eq. (8). However, if the thrust stand is tilted by an angle θ_z, defined in Fig. 6, an additional term appears:

$$\theta_{ss} = \frac{F_t L_t}{k} + \frac{\theta_z}{((k_s/mgL_{cm}) - 1)} \tag{16}$$

Inverted pendulum thrust stands yield large deflections for a given force F_t when mgL_{cm} is comparable to k_s. But, this can also make the second term in Eq. (16) large, so θ_z must be constant for the thrust stand response to be repeatable. Most inverted pendulum thrust stands therefore incorporate active control of the inclination. Counterweights can also be used to move the center of mass closer to the pivot point, which eliminates this effect [31]. However, it also eliminates the advantages of using the gravity torque to improve sensitivity and generally results in larger thrust stands.

Compact inverted pendulum thrust stands are also particularly vulnerable to heat absorbed from the thruster, which can alter the spring constant and cause zero and gain shifts. Thermal shrouds and active cooling of critical thrust stand components are essential to minimize thermally induced drift in thrust measurements. Finally, as in all pendulum thrust stands, the sensitivity is dependent on the stiffness of all components of the thrust stand, including electrical leads and propellant tubing necessary for thruster operation. Care

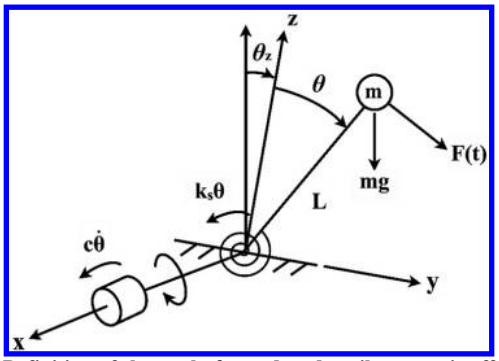

Fig. 6 Definition of the angle θ_z used to describe a z axis offset from gravity.

must be taken in the mechanical design to ensure that the stiffness of these components does not change during operation.

1. Mechanical Design

Inverted pendulum thrust stands can be built with a single linkage like the idealized schematic in Fig. 1 [25]. However, most inverted pendulum thrust stands use parallel linkages to keep the thruster oriented horizontally throughout their range of motion [26,30–35]. All movement of the thrust stand is mechanically blocked except for straight-line deflection parallel to the thrust vector, which yields a number of advantages. Significant rotation of the electric thruster is undesirable where plume diagnostics take place simultaneously with thrust measurement. In addition, the thruster center of mass can be positioned anywhere on the movable upper platform without significant impact on measurement accuracy. Finally, magnetic coupling between the electric thruster and the earth's magnetic field should not result in significant moments about the pendulum arm. These advantages come at the cost of additional complexity. A parallel linkage thrust stand has roughly four times as many moving parts and joints when compared to a simple inverted pendulum configuration. The additional joints increase the spring stiffness of the thrust stand, requiring additional pendulum height or mass to match the sensitivity of a single-linkage stand.

An example of an inverted pendulum thrust stand developed at the NASA John H. Glenn Research Center is shown in Fig. 7 [26]. Parallel linkages (side plates with flexures connecting the upper movable platform to the fixed bottom plate) share the vertical load and maintain the top plate in a horizontal orientation. Many electric thrusters have thrust-to-weight ratios less than 1/500. Consequently, the arm of the thrust stand is primarily stressed in compression, supporting the thruster weight. Although it is desirable to have highly flexible pivots in the pendulum, they must be stiff enough to avoid buckling under the weight of the thruster and resist handling loads during installation. Fixed mechanical stops are provided to limit thrust stand deflection and prevent accidental collapse. For high sensitivity, the pendulum arm should be long enough to yield a gravity torque for a given mounted weight that approaches the spring torque. To remain stable, however, the gravity torque must not exceed the spring torque. In practice, the thrust stand sensitivity is generally fine-tuned by adding ballast to the upper platform or an auxiliary spring to increase the effective spring constant.

Up to 5 mm of displacement is measured with an LVDT. The displacement signal is processed by a PID controller, which drives an electromagnetic actuator coil to damp high-frequency motion. The damper signal is carefully balanced to ensure that it contains no dc bias. The low-frequency portion of the LVDT output is recorded as the thrust signal. Alternatively, the thrust stand can operate in null mode, described in detail in Sec. III.E. In this configuration, the PID controller uses the low-frequency LVDT output to drive current to a second water-cooled null coil, which holds the thrust stand at a given set point. The null coil current serves as the thrust signal.

A high-sensitivity gravitational inclinometer ("tilt sensor") mounted on the bottom plate monitors thrust stand inclination changes, which are often caused by facility distortions during pumpdown or thermal distortions during operation. The inclination is automatically corrected by raising or lowering the rear of the thrust stand relative to a pivot point near the front using an actuator (typically a motor-driven screw) located at the end of a long pivot arm. The thruster is thermally isolated from the thrust stand by a water-cooled mounting post. The entire thrust stand is contained within a temperature-regulated water-cooled enclosure (not shown), except where the cooled mounting post protrudes. Thrust stands of this type have been used to test thrusters ranging from 100 kW Hall engines with mass in excess of 100 kg [32] down to 300 W Hall thrusters with a mass of 0.9 kg [30].

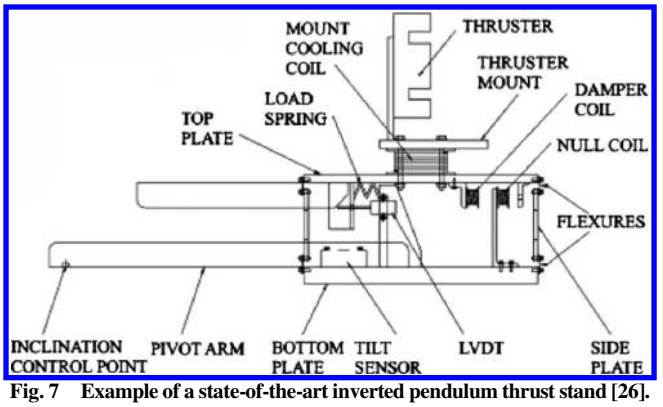

Fig. 7 Example of a state-of-the-art inverted pendulum thrust stand [26].

2. Thrust Stand Performance

One advantage of inverted pendulum thrust stands is that the sensitivity can be easily tuned by adding or removing ballast or changing the auxiliary spring. Vibration transmitted to the thrust stand from the facility is generally the dominant disturbance that limits thrust stand resolution. Vibrations can be attenuated by isolating the thrust stand and by choosing a natural frequency much less than the frequency of vibrations. Full-scale deflection is often chosen to be at least two orders of magnitude larger than expected vibrational noise within the vacuum facility. Assuming a noise amplitude of 0.025 mm, a full-scale deflection choice of 2.5 mm would result in 1% noise.

For angles less than 5 deg, inverted pendulum thrust stand deflection is assumed to be linearly proportional to applied thrust [Eq. 5]. The measurement error due to nonlinearity is usually much less than other errors introduced by zero drift and vibration. End-to-end calibration, from thrust stand to data recorder, is easily performed by applying known loads to the pendulum, as described in Sec. IV. Another advantage of parallel linkages in inverted pendulums is that the calibration force can be applied at any point on the rigid platform on which the thruster is mounted. With a single pendulum arm, the calibration forces must either be applied at the same distance from the pivot as the thrust forces or the location of the calibration forces relative to the thrust forces must be known accurately to scale the resulting torques.

Long-term drift in thrust stand response is generally due to thermal effects or changes in the stiffness of parasitic spring elements. Both can be controlled with careful thermal design and choice of materials. Sections IV and V discuss methods for managing drift in calibrations and measurements.

Thrust stand sensitivity, noise, and response time are related through the pendulum dynamics reviewed in Sec. II.B. One way of expressing sensitivity based on the preceding equations is as the maximum linear deflection x_{FS} in response to full-scale thrust F_t, measured at the distance of load application from the pivot L_t, or

$$\frac{x_{\mathrm{FS}}}{T} = \frac{L_t^2}{k} \tag{17}$$

Assuming that the moment of inertia is $I \approx L_t^2 M_t$, where M_t is the thruster mass, the natural frequency can be expressed as

$$\omega_n = \sqrt{\frac{k}{L_t^2 M_t}} = \sqrt{\frac{(F_t/W)g}{x_{\mathrm{FS}}}} \tag{18}$$

where $W = M_t g$ is the weight of the thruster. The thrust-to-weight ratio (F_t/W) of electric thrusters is usually much less than one. For arcjet thrusters, (F_t/W) is typically 1/200; for Hall thrusters, (F_t/W) is typically 1/300; and for gridded ion thrusters, (F_t/W) is typically 1/600 [30,36]. The characteristic response time for a critically damped thrust stand to settle is approximately one period:

$$\tau_n = 2\pi/\omega_n = 2\pi\sqrt{\frac{x_{\mathrm{FS}}}{(F_t/W)g}} \tag{19}$$

If a Hall thruster were to be tested that had a thrust-to-weight ratio of 1/300, the expected settling time would be approximately 1.7 s.

The actual natural period will be somewhat longer than this, due to the additional mass for the thrust stand top plate, mounting brackets, tubing, and electrical cables. A response time of several seconds is usually adequate for most performance tests, where thermal equilibrium of the thruster may not be reached for many minutes. If necessary, response time can be improved by selecting a smaller full-scale deflection x_{FS}, assuming vibration noise levels are acceptable.

Properly designed inverted pendulum thrust stands like that shown in Fig. 7 have demonstrated excellent performance over a range of thrust levels. For example, thrust levels ranging from 5 to 20 mN were measured for a 0.3 kW Hall thruster with an estimated uncertainty of $\pm 1.5\%$ [30]. Thrust levels up to 2.3 N were measured for a 50 kW Hall thruster with an uncertainty estimated to be $\pm 2\%$ [37].

C. Hanging Pendulum Balances

Thrust stands based on hanging pendulums are conceptually simple and easy to use in principle. In their simplest form, conventional hanging pendulums consist of a vertical arm attached to a top pivot or flexure and a thruster mount or platform at the bottom. They are inherently stable because the gravity torque always acts to restore the pendulum to the null position. In fact, gravity is generally the dominant restoring force, so they have proven to be the least susceptible to zero drift caused by changes in flexure stiffness. However, because electric thrusters have low-thrust-to-weight ratios, the deflections of hanging pendulum thrust stands are often very small, which can complicate their design and use.

1. *Mechanical Design*

The primary challenge in mechanical design is to achieve deflections for the expected thrust range that are measurable with adequate resolution. Because the effective spring constant in hanging pendulum stands is generally dominated by the weight term (Eq. 6), the main design approach to increasing sensitivity is to lengthen the pendulum arm, as is apparent in Eq. (14). Therefore, more sensitive stands typically require large-diameter vacuum facilities. Mechanical linkages that magnify the deflection of the arm and counterweights have also been employed to improve sensitivity [19]. Alternatively, sensors such as laser interferometers that are capable of measuring small deflections with high resolution are used [5,13]. In this case, vibration isolation or compensation, active inclination control, and careful thermal design are required to minimize these disturbances to the small thrust signal.

An example of a state-of-the-art hanging pendulum thrust stand is the nanobalance, shown schematically in Fig. 8, which was developed for microthruster applications by Thales Alenia Space Italia in cooperation with the Italian National Metrology Institute and Polytechnic of Turin [5,13]. This stand consists of two Beryllium Copper (BeCu) plates that hang from BeCu flexures attached to a rigid block of Zerodur©, which is a material with a very low coefficient of thermal expansion. The microthruster to be tested is mounted on one of the plates and an identical dummy mass on the other. Both plates are assumed to have the same dynamical behavior, so they respond in the same way to common-mode vibrations from the environment. The displacement of one plate relative to the other is then measured as a thrust response that is free of environmental vibrations. Extensive vibration isolation on the stand and the vacuum facility is also used to minimize disturbance inputs. Two spherical mirrors mounted on the plates form an optical cavity for a Fabry–Pérot laser interferometer, allowing very sensitive measurements of the relative displacement (described briefly in Sec. III.A). Two calibrated actuators (voice coils) that produce a variable force on a permanent magnet by the field from an electromagnet are used to calibrate each of the pendulums in situ. The force produced by these actuators was independently measured [13].

Like all pendulum thrust stands, this one is subject to zero drifts caused by changes in the inclination of the mount from which the pendulum plates hang and thermal effects. The nanobalance incorporates piezoactuators that level the stand based on feedback from an inclinometer mounted on the Zerodur frame. Temperature control and a careful choice of materials were used to minimize thermal drift, and residual drifts in the signal were corrected with polynomial fits to the measured temperature [13].

2. *Thrust Stand Performance*

Using these techniques allows hanging pendulum thrust stands to achieve very high performance. For example, the nanobalance has demonstrated a linear response (in terms of frequency shift measured with the Fabry–Pérot interferometer) over thrust levels up to 1 mN. The thrust stand sensitivity in terms of deflection for a given force was only 140 pm/μN, but a resolution of 0.1 μN was enabled by the high spatial resolution of the interferometer. The measurement accuracy was 0.65 μN (based on random noise characterized over a period of 10000 s) $+1\%$ of reading. A noise floor spectral density of less than 0.1 $\mu\text{N}/\sqrt{\text{Hz}}$ between 0.1 and 1 Hz (and less than 1 $\mu\text{N}/\sqrt{\text{Hz}}$ down to 1 mHz) was measured [13]. Larger hanging pendulum thrust stands have demonstrated performances similar to inverted pendulum stands for thrust levels up to several newtons [19].

D. Torsional Pendulum Thrust Stands

Unlike both the hanging and inverted pendulum thrust stand configurations, an ideal torsional pendulum's rotational axis is

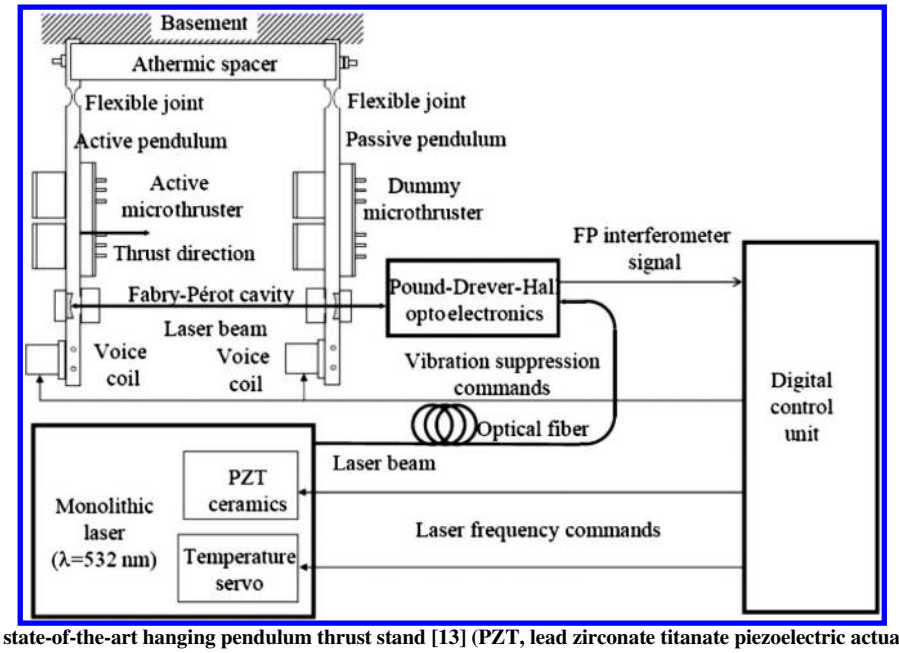

Fig. 8 Example of a state-of-the-art hanging pendulum thrust stand [13] (PZT, lead zirconate titanate piezoelectric actuator; FP, Fabry-Pérot).

parallel to the gravity vector, making its response independent of thruster mass. Torsional pendulum thrust stands, also called torsion balances, are well suited for thrusters that are either changing in mass or for testing in facilities that must accommodate a very large range of thruster weights. Torsion balances have shown very high sensitivity, making them particularly useful for micropropulsion applications. Torsional thrust stands are inherently more stable than inverted pendulum thrust stands [7] and offer a balance between high-thrust measurement sensitivity and low environmental noise sensitivity [19,38].

Because low-thrust measurements require long beams, torsional thrust stands may be difficult to accommodate in smaller vacuum chambers. This is especially true for the optimal symmetric arm configuration. Although asymmetric configurations are possible (such as a "swinging-gate" configuration [12]), this approach can lead to induced coupling modes excited by facility vibrations. Gravity can affect measurements under two conditions: 1) when the vertical rotation axis is offset from the gravity vector, and 2) when the center of mass does not lie on the vertical rotation axis. In the first case, when the offset angle is positive, the system is stable because the torque works with the spring as a restoring force. As the offset angle grows more negative, the torque will resist the spring force and, at large enough negative angles, lead to instability. Two design variables can be adjusted to reduce the magnitude of gravity torques [8]: the distance of the center of mass from the rotation axis and the offset angle. It is generally easiest to change the distance of the center of mass from the rotation axis. Counterweights are often used on the side of the beam opposite the thruster to place the center of mass of the beam system very near the axis of rotation [8,9,14–16,24,28].

Torsional thrust stands can resolve thrust levels from hundreds of nanonewtons to a few newtons [16,22,23,28], spanning a large range of thrusters such as field emission electric propulsion, pulsed plasma thrusters, gridded ion thrusters, and Hall thrusters.

1. *Mechanical Design*

Figure 9 shows a typical torsional thrust stand design [8]. Torsional thrust stands use a long beam attached at two flexural pivots where torsion springs provide a restoring torque, ideally parallel to the gravity vector. Thrust measurements are obtained by determining the angular deflection of the beam. The linear displacement $x(t) \simeq L_{\mathrm{pm}}\theta(t)$ at a specified position along the beam L_{pm} is measured. In this example, deflections of up to a few millimeters are measured with an LVDT. An electromagnetic damper provides active damping using a PID controller. Two motor-driven screws on orthogonal arms provide active leveling to compensate for shifts in the thrust stand base that occur during facility pumpdown.

2. *Thrust Stand Performance*

Torsional thrust stand sensitivity depends on a number of design choices, including the torsion spring constant, length of the thrust stand beam, and measurement distance from the axis of rotation. As in the thrust stands described previously, the angular deflections are generally limited to less than about 5 deg so that the measured displacement can be linearly related to thrust. The typical thrust stand resolution is better than 1 μN for steady-state forces and less than 1 μN · s for impulse measurements [8]. Even higher resolution (less than 0.03 μN) has been reported [14]. Yang et al. reported resolutions of 0.47 μN · s for impulse bits up to 1350 μN · s and 0.09 μN for steady-state thrust values up to 264 μN [15]. Several torsional thrust stands have demonstrated frequency-dependent noise floors that meet the demanding requirements of the ST7/LISA Pathfinder mission (see Fig. 5, for example, which displays the noise floor measured with the thrust stand shown in Fig. 9 [8]). Overall thrust stand accuracies of ±0.5 μN for steady-state thrust levels from 1 to 100 μN [8] and impulse accuracies of 2.1 μN · s for an impulse range of 20–80 μN · s and 0.7 μN · s for an impulse range of 1–10 μN · s [2] have been measured.

E. Steady-State Null Balances

The goal of steady-state thrust measurement is to determine an unknown force in a laboratory environment and track slowly developing variations in that force. A steady-state null balance accomplishes this by applying a control force to cancel thrust stand deflection caused by the unknown force [15,26,31]. When the deflection has been nullified to zero, the control force is assumed to equal the unknown force.

Conventional thrust stands based on spring–mass systems must be carefully sized so that the load spring is capable of absorbing the maximum expected force. However, an excessively stiff load spring could result in reduced force measurement resolution. With a null balance, the control force absorbs all of the unknown force, and the system spring constant is much less critical. In addition, conventional thrust stands based on spring–mass systems, by necessity, allow the thruster to move. The exact position and pointing of the thruster within the test facility is not well controlled, which may complicate other diagnostics such as plume or thrust vector measurements. With a null balance, the thruster position is strictly determined by the system set point, except during brief thrust transients.

The mechanical configuration of the null balance thrust stands can be very similar to spring–mass-type thrust stands. Other than the addition of a force actuator, both stands have many of the same components, including a position sensor. However, the overall system design of a null balance is very different. Although spring–mass thrust balances typically operate open loop, a null balance uses a tuned feedback loop for stable operation. A PID control system is generally implemented in software [31] or hardware [15,26] to regulate the actuator control force. The null balance control system must keep the position sensor at the exact set location under steady test conditions. Precise knowledge of the control force is necessary because this is assumed to equal the unknown force to be measured.

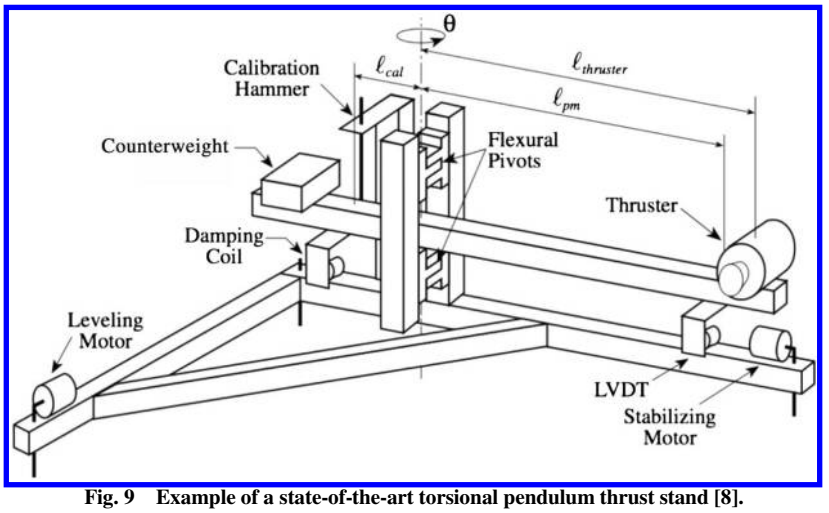

Fig. 9 Example of a state-of-the-art torsional pendulum thrust stand [8].

Electromagnetic actuators similar to those used as active dampers are typically employed, and the solenoid current is sensed as a measure of actuator force. Active cooling of the force actuator may be required at higher-thrust levels because of heat generated in the coil. Null balances are calibrated in the same way as conventional thrust stands, as described in the next section.

IV. Calibration

Calibration serves three primary purposes. First, the calibration process produces the relationship between deflection or sensor output and thrust or impulse. Second, the accuracy, precision, and repeatability of a thrust stand are determined by repeated application of known forces or impulses, so it is an integral part of the error quantification. Finally, comparison of measured response with the expected theoretical response can reveal systematic problems that would bias the measurements if uncorrected.

A. Application of a Known Force

Laboratory testing of an electric thruster often requires complex interfaces between the thruster and the test facility. Electric current, instrumentation, and various propellants must be provided to the thruster through these interfaces: all of which contribute elastic stiffness and affect the static equilibrium. Although these contributions could be characterized individually and summed to calculate the total effective spring constants that determine thrust stand sensitivity [15], it is much more practical to perform an end-to-end calibration of the entire thrust stand installation, where all dynamic and static forces are characterized simultaneously. The calibration process is typically performed with the entire installation fully prepared to test, under vacuum, and only minutes before startup of the electric thruster. Calibration involves applying known forces F_{cal} at a point L_{cal} from the pivot and monitoring the change in position at L_{pm} to determine the thrust stand sensitivity:

$$S_{\text{cal}} = \frac{\Delta x_{\text{ss}}}{F_{\text{cal}}} = \frac{L_{\text{pm}} L_{\text{cal}}}{I\omega_n^2} \tag{20}$$

To calculate the steady-state thrust of a thruster from a measured displacement Δx_{ss}, this sensitivity must be scaled by the difference in distances from the pivot at which the calibration and thrust forces are applied:

$$F_t = \frac{(L_{\text{cal}}/L_t)}{S_{\text{cal}}} \Delta x_{\text{ss}} \tag{21}$$

The uncertainty in the ratio L_{cal}/L_t must be included in the total thrust uncertainty estimate. If the calibration forces are applied in the same location as the thrust forces, the ratio $L_{\text{cal}}/L_t = 1$ and the thrust force can be determined directly from the calibration curve for a given Δx_{ss} measurement. The sensitivity of null balance thrust stands is calibrated by measuring the force actuator coil current, rather than pendulum displacement, as a function of applied force.

Calibration forces can be applied in a number of ways. One common approach is to load and unload weights with known masses on a flexible fiber that passes over a pulley and attaches to the pendulum, as illustrated in Fig. 10. The fiber must be carefully aligned with the thrust vector, and the pulley must be designed with minimum static and dynamic friction so that it transmits all of the force from the weights to the stand. An advantage of null balances is that they are unaffected by dynamic friction. An example of the thrust stand response to this kind of calibration is plotted in Fig. 11. These data were obtained with an inverted pendulum thrust stand similar to that shown in Fig. 7. In this case, four calibration weights were hung from a fine chain that passed over a pulley and attached to the rear of the moveable upper platform. The other end of the chain was attached to a cylinder mounted behind the pulley that could be turned with a small dc motor to raise the weights on the cylinder side of the chain loop, removing the force from the thrust stand. The position of the takeup cylinder was measured with a potentiometer. The change in

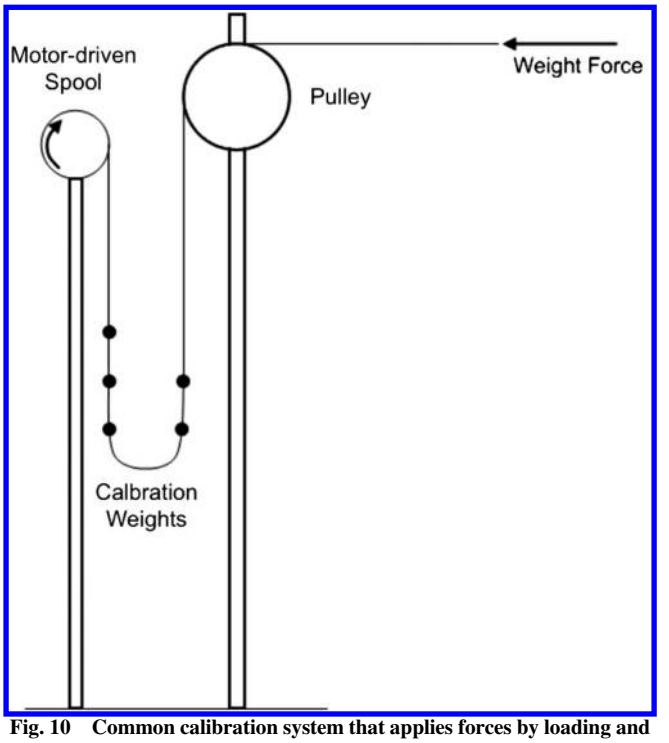

Fig. 10 Common calibration system that applies forces by loading and unloading weights with known masses [31].

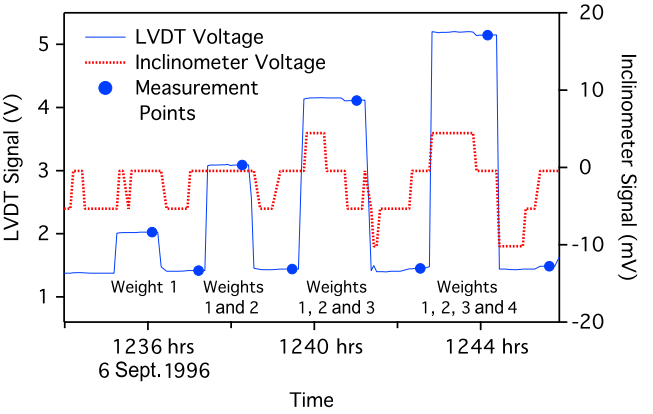

Fig. 11 Thrust stand response to application of known forces.

the LVDT signal, which was proportional to the thrust stand displacement, with application of one, two, three, and all four weights was measured. The position of the balance is sensitive to the inclination of the base, so this was measured with an inclinometer and actively controlled using a dc motor-driven screw to raise or lower one end of a cantilever beam on which the thrust stand was mounted. The inclinometer output voltage was used as the feedback signal to a software proportional controller that controlled the motor. Application of the weights caused small shifts in the inclination, as shown by the inclinometer signal in Fig. 11, which were then corrected by the controller.

As in this example, the force from the calibration weights is often stepped up and down incrementally using a remotely operated mechanism. The transducer signal is measured after applying weights and after removing them (the thrust stand zero), as shown by the solid circles in Fig. 11. These measurements are often averaged over a number of samples to obtain a good estimate of the mean value, particularly if the transducer signal is noisy. The thrust stand response is defined as the difference between the signal with weights and the zero measured immediately afterward. This approach automatically corrects for any drift in the thrust stand zero. The calibration process should be designed so that the calibration weights span the range of expected thrust values and are evenly distributed across the range.

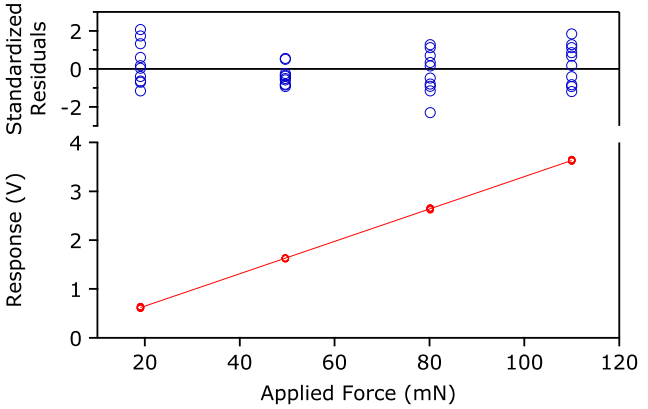

Fig. 12 Calibration data relating thrust stand deflection in terms of LVDT sensor output to applied force with linear fit and standardized residuals.

Figure 12 shows an example of a calibration curve constructed from $n = 40$ observations of thrust stand response for given input forces similar to those plotted in Fig. 11. The response is modeled as a linear function of the applied forces

$$x_i = \beta + \mathcal{S}F_i + u_i \tag{22}$$

where the x_i are the measured responses to input forces F_i, $\mathcal{S}$ in this case corresponds to the sensitivity of the balance, and the u_i are random disturbances. A finite force has to be applied to overcome static friction, so a plot of deflection vs force will typically exhibit a negative intercept. If the linear fit to the data is forced to go through zero, it will introduce additional error. The intercept β should be estimated from the data. The disturbances are assumed to be normally distributed with a mean of zero and a common variance of σ_x^2. The input forces are assumed to be known without error, so the calibration method must be designed so that the uncertainty of the input loads is much less than that of the stand response. Standard curve-fitting routines can be used to perform a least squares analysis to determine b and S_{cal}, which are estimates of β and $\mathcal{S}$ that minimize the sum of squared residuals:

$$\sum_{i=1}^{n} u_i^2 = \sum_{i=1}^{n} (x_i - \beta - \mathcal{S}F_i)^2 \tag{23}$$

These regression parameters then yield predicted values of the response for given inputs

$$\hat{x}_i = b + S_{\text{cal}}F_i \tag{24}$$

The calibration data can be used to calculate an unbiased estimate of the variance σ_x^2 of the random disturbances

$$\sigma_x^2 \simeq s_x^2 = \frac{\sum_{i=1}^{n} (x_i - b - S_{\text{cal}}F_i)^2}{n-2} \tag{25}$$

The standard deviation s_x is a way to characterize the variability in response with fixed input and plays a key role in the error estimate, discussed in more detail in Sec. VI. The standardized residuals $e_i/s_x = (\hat{x}_i - x_i)/s_x$ are also plotted in Fig. 12. Residual plots are a very powerful way to evaluate the quality of a fit [39]. In general, if the assumed model is correct, the standardized residuals will fall uniformly between -2 and $+2$ and will be randomly distributed around zero. A systematic pattern of variation in the residuals can indicate a deviation from linear behavior or other violations of the assumptions on which the least-squares analysis relies. Another parameter often used in evaluating fits is the square of the correlation coefficient:

$$R^2 = 1 - \frac{\sum (x_i - \hat{x}_i)^2}{\sum (x_i - \bar{x})^2} \tag{26}$$

where $\bar{x}$ is the mean of the measured responses. This is a measure of the proportion of total variability in the x_i that can be explained by the F_i. However, it is only a measure of correlation, and a high value does not mean that the data have been well fit or that the calibration curve will yield results with low uncertainty [39]. To illustrate this, Anscombe [40] generated four hypothetical datasets, with each yielding the same summary statistics for a linear least-squares fit (including the same value for R^2). However, three of the four datasets were clearly not well represented by the linear fit, deviating from the linear model due to different pathologies. Careful examination of the residuals can help avoid these pitfalls and is recommended for high-quality thrust measurements. For example, a lack of linearity or repeatability apparent in the residuals typically indicates a mechanical problem with the thrust stand installation, such as dragging or unintentional contact with something as the thrust stand deflects, which should be corrected before making thrust measurements.

B. Application of a Known Impulse

Pendulum thrust stands can also be used to make impulsive measurements but must be calibrated to characterize the response over the appropriate range of impulse bits. Thrust stands used in impulse measurements are typically underdamped pendulums that are allowed to oscillate at their natural frequency after an impulse perturbation. Hanging or inverted pendulums can be used, but torsional balances offer improved sensitivity. Because the free response of the thrust stand to the impulse is measured, these are not null balances. Active electromagnetic dampers may be used to reduce vibrations from the facility, but they are turned off before making impulse measurements [2,7].

Although thrust stand parameters such as the effective spring constant and natural frequency or moment of inertia can be measured to calculate the sensitivity [7,15], calibration is usually accomplished by applying known impulses $I_{\text{bit,cal}}$ at a point L_{cal} from the pivot and inferring the sensitivity from a change in the dynamic response of the swinging arm (such as initial velocity, peak amplitude, or full range of motion) similar to the method outlined previously for thrust measurements. For example,

$$S_{\text{cal}} = \frac{\Delta\dot{x}(0)}{I_{\text{bit,cal}}} = \frac{L_{\text{pm}}L_{\text{cal}}}{I} \tag{27}$$

assuming an impulsive force at $t = 0$. As in thrust measurements, this sensitivity must be scaled by the difference in distances from the pivot at which the calibration and thrust forces are applied to calculate the impulse from a measured change in velocity $\Delta\dot{x}(0)$; for instance,

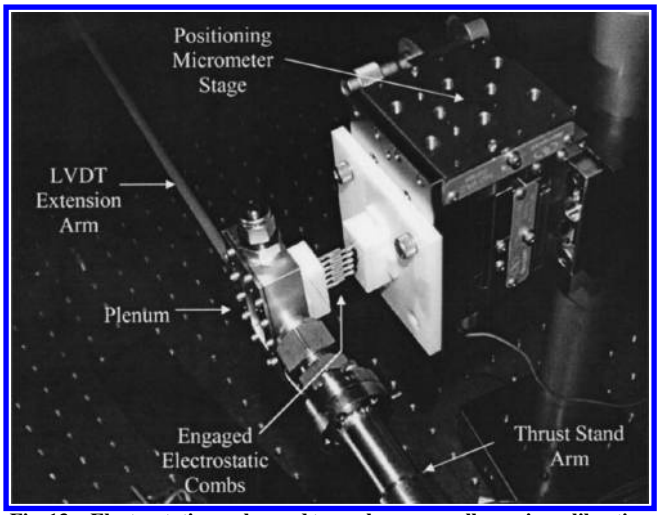

Fig. 13 Electrostatic combs used to apply very small, precise calibration impulses [42].

$$I_{\text{bit}} = \frac{(L_{\text{cal}}/L_t)}{S_{\text{cal}}}\Delta\dot{x}(0) \tag{28}$$

Typical calibration methods can be broken down into either contact or noncontact methods. Several contact calibration methods involve the swinging of known masses [4,41] or the use of impact pendulums [2] or impact hammers [8]. Noncontact methods include calibration using electrostatic forces between planar electrodes [14], free molecular gas flow from underexpanded orifices [9], electrostatic combs [24], and electromagnetic coils [17]. Of these methods, we recommend piezoelectric impact hammers and electrostatic combs, which are common practice and provide precise, controllable impulses over a broad range.

Electrostatic combs (ESCs) like those shown in Fig. 13 are known for their versatility because they can provide both a steady-state force as well as a wide range of impulses. ESCs consist of a set of interlocking noncontacting combs separated by a small gap. One set of the pair is placed on the moving part of the stand (usually the grounded set), and the other is mounted on the fixed part of the stand and aligned with the moving combs. The attractive force provided by the combs is a function of the applied voltage, the geometry, and the number of comb pairs in a set [43]. Unlike electrostatic actuators using planar electrodes [14], this comb geometry is independent of the gap or engagement distance between the combs. This has two major implications for impulse balance calibration. First, it does not require that the location of the stand, and therefore the engagement distance, be known with great accuracy. Second, even though the engagement distance is changing slightly as the stand oscillates, the force applied by the combs does not change throughout the stand's motion.

By accurately controlling the amount of charge, or voltage, on the combs as well as the time that the charge is applied, a well-known impulse can be created. ESCs can accurately produce forces from tens of nanonewtons [42] to tens of millinewtons [24] with errors typically less than 1%. By varying the pulse width and amplitude of the applied voltage, Pancotti et al. demonstrated impulses ranging from 0.01 to 20 mN · s, which produced responses of a torsional thrust balance that were linear to within 0.52% [24]. The capacitance of the combs may lead to voltage overshoot at the beginning of the pulse. Although this might not be an issue for longer pulse times, voltage overshoot from very short pulses may induce errors [24]. It is important therefore to understand the dynamic characteristics of the pulse-forming system and design the circuit to minimize overshoot.

As with any calibration system, the calibration mechanism itself must be well calibrated so that the uncertainty in the applied impulses is very low, which is a key assumption of the linear least-squares analysis. The force generated by electrostatic combs as a function of applied voltage is typically measured by mounting the comb assembly on a microbalance scale that has been calibrated with National Institute of Standards and Technology (NIST)-traceable standards. The impulse delivered by a pulsed comb system is calculated by integrating the force over the pulse width.

Piezoelectric impactors are commercially available in a variety of shapes and sizes, and they are generally precalibrated. The typical procedure for impulse balance calibration is to strike the stand with the force transducer while recording the output voltage from the transducer. This output voltage is calibrated to correspond to a force, and integrating over time yields a total impulse. The force transducer can be mounted on a swinging pendulum arm that, when released, will strike the stand. The magnitude of impulses applied in this manner can be varied by adjusting the pendulum release height and the striking material. Typically, the cocked angle and the release trigger are controlled by an electromagnetic actuator [8]. Forces ranging from 0.5 to 100 N with errors of ±2% can be achieved with this method [44]. Calibration hammers can also be driven with a servomotor, which can provide very accurate control of position and velocity, as well as improve the accuracy of the applied impulse. Servocontrolled swing arms have been used to produce impulses ranging from 10 to 750 mN · s and generated a thrust stand response that was linear to within 0.5% over that range [24].

For piezoelectric hammers, a proper calibration should be performed either by the manufacturer or preferably in-house under the conditions the force transducer would be used. To calibrate a force transducer, a free suspended reference mass with an attached accelerometer can be used [24]. Beyond the calibration itself, other factors including strike location, digitization, and integration all have to be carefully conducted in order to properly track errors and determine the total accuracy of the impulse calibration system.

The known calibration impulse will perturb the natural motion of the stand and cause it to ring or oscillate at its natural frequency. Figure 14 shows a plot of LVDT voltage as a function of time for a torsional balance that has experienced an impulsive perturbation. The impulse causes the stand to deflect with an initial velocity $\Delta\dot{x}(0)$ and a maximum range of travel, defined as the difference between the first peak and the first valley in the oscillatory response. These parameters can be estimated by fitting a damped sinusoid (for underdamped pendulums) to the data. The analysis of linear fits outlined previously can be extended to nonlinear fits such as this. In practice, there is often a small amount of background motion or drift that must be subtracted to determine the change in motion due to the impulse. In this case, a damped sinusoid is also fit to the position history before the impulse and the response is defined as the difference between that and the motion after the impulse [8]. In a careful study of the variance associated with various fitting approaches, Koizumi et al. [2] found that the noise was predominantly at the natural frequency of the stand and could be distinguished from the thruster impulse by fitting the data over a range of $(-2\tau_n, 2\tau_n)$ with a function of the form

$$x(t) = \begin{cases} A_N \sin(\omega_n t) + x(0)\cos(\omega_n t), & t \le 0 \\ A_F \sin(\omega_n t) + A_N \sin(\omega_n t) + x(0)\cos(\omega_n t) & t > 0 \end{cases} \tag{29}$$

where A_N is the amplitude of the noise, and A_F is the amplitude due to the impulse. Their stand was minimally damped, so they did not include a damping term. An exponential decay representing damping could be added to the fit for stands with greater damping [see Eq. (10)].

If the impulse applied to the stand is known accurately, a good correlation between either the initial velocity or the maximum range and the applied impulse can be determined. An example calibration curve obtained with data similar to that shown in Fig. 14 is plotted in Fig. 15. Figure 16 displays a calibration curve for the torsional balance shown in Fig. 9 based on measurements of the initial velocity change due to impact hammer impulses. In both of these examples, the transducer signal is not translated into actual displacement or velocity. As long as it is linearly proportional to the motion, the transducer signal can serve as the parameter that is correlated with thrust or impulse. Data such as these can be fit using a linear least-squares analysis to obtain an estimate of the sensitivity S_{cal}. The same recommendations for the design and analysis of linear calibration curves listed previously should be followed with impulse calibrations as well.

The thruster impulse must approximate a true impulsive load: $F(t) = I_{\text{bit}}\delta(t)$. In practice, a linear response can be obtained for finite pulse lengths, as long as they are much shorter than the natural

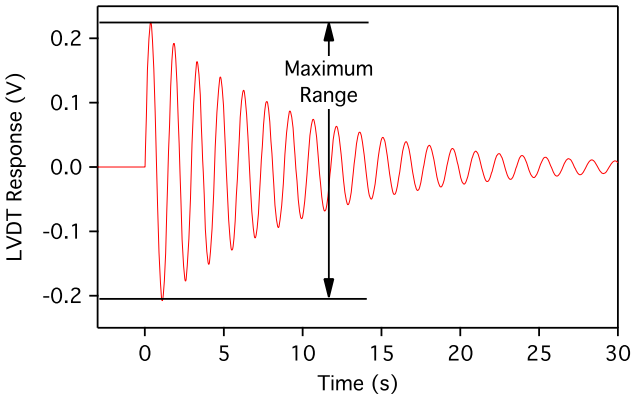

Fig. 14 Displacement sensor (LVDT) response as a function of time from an applied impulse.

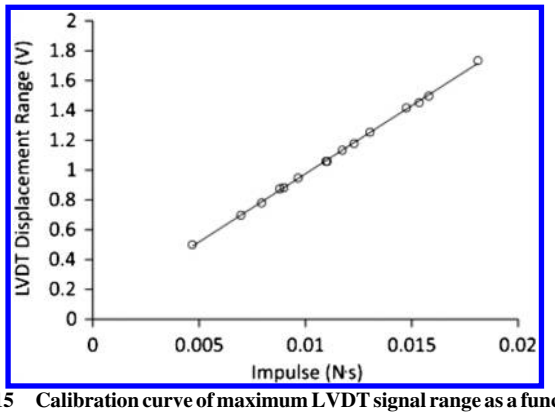

Fig. 15 Calibration curve of maximum LVDT signal range as a function of impact hammer impulse.

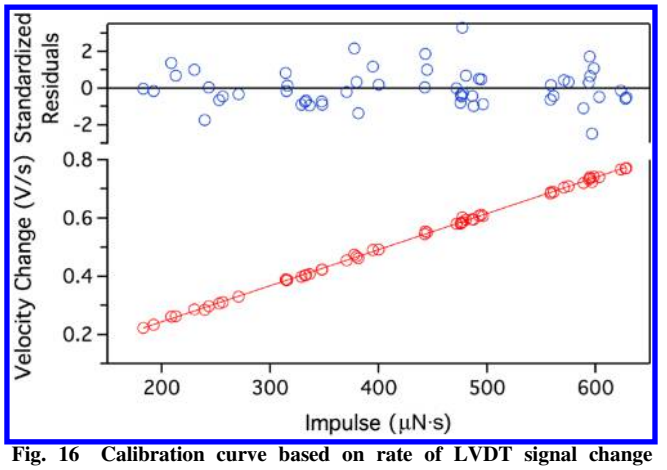

Fig. 16 Calibration curve based on rate of LVDT signal change (proportional to velocity) vs. impulse.

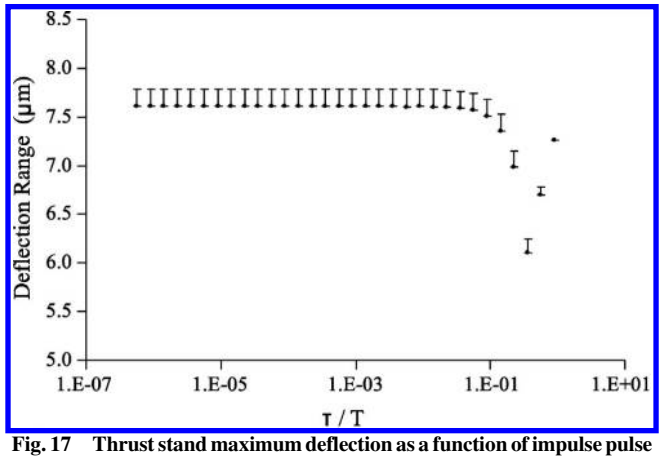

Fig. 17 Thrust stand maximum deflection as a function of impulse pulse width normalized by the natural period of the balance [21].

frequency of the stand. Figure 17 shows a range of travel for varying impulse times τ divided by the stand's natural period τ_n. As impulse times become greater than about 1/10, the stand's natural period the results become nonlinear. Therefore, we recommend that known calibration impulses be applied with pulse widths much less than the period of the stand.

V. Measurement Procedure and Data Reduction

A. Thrust

Data reduction for steady-state thrust measurements involves a straightforward application of the calibration curve to calculate thrust. To obtain the most reliable single point measurement of steady-state thrust, the following procedure is recommended. First, determine what level of error in the thrust measurement is tolerable. For early development activities, relatively high uncertainty may be acceptable, whereas much greater precision and accuracy might be required for characterization of thrust for a flight program. Perform a minimum of 10 calibrations to generate a calibration curve with small random errors and examine the curve for signs of systematic bias and short-term drift. Compare to previous calibrations for signs of long-term drift. If the calibration indicates that the thrust stand is performing as required, start the thruster and allow it to reach thermal equilibrium and steady operation. Obtain an adequate number of measurements of the thrust stand transducer signal to calculate a mean value with a sufficiently small standard error. Turn off the thruster power and flow rate, and obtain measurements to characterize the zero (no load) transducer output. The difference between the transducer output with the thruster on and under no load conditions will be considered the response for that operating point. Repeat this measurement cycle if possible to characterize the repeatability of thrust measurements. Perform a minimum of 10 calibrations after thruster operation to monitor shifts in the thrust stand sensitivity. If the calibrations taken before and after the thrust measurement indicate that the thrust stand response is stable (i.e., if differences in the calibrations result in contributions to the total error estimate that meet the requirements for that particular thruster), compute the thrust from the measured response.

An example of the transducer signal obtained with an ion thruster like those used on NASA's Dawn mission is plotted in Fig. 18 [45]. The sudden drop in LVDT voltage is associated with turning off the high voltage to the engine. The main flow is shut off shortly after that, and small changes in the LVDT signal are apparent as the feed system lines downstream of the valve are evacuated. The zero signal is measured when the gas flow has stopped. Variations in the LVDT signal after that reflect the start of a calibration sequence. The thrust generated by the mass flow through the engine without power is often significant, particularly for electrothermal thrusters such as arc jets, and special measures may be required to properly characterize it. Thrust stands are often subject to rapid thermal transients when the engine is first turned off, and the thrust stand zero should be measured before these transients cause significant drift. This may necessitate the use of a flow shutoff valve very near the engine to minimize the blowdown thrust transient.

Time-resolved thrust measurements may be obtained from the time history of the transducer signal during thruster operation if the thrust stand zero is sufficiently stable. The error can be bounded by measuring the zero before and after thruster operation; if the time-dependent variation in the zero can be determined, a correction may be applied to the data. Measurements of the temperature of the thrust stand components most susceptible to thermal effects may help guide the correction [13].

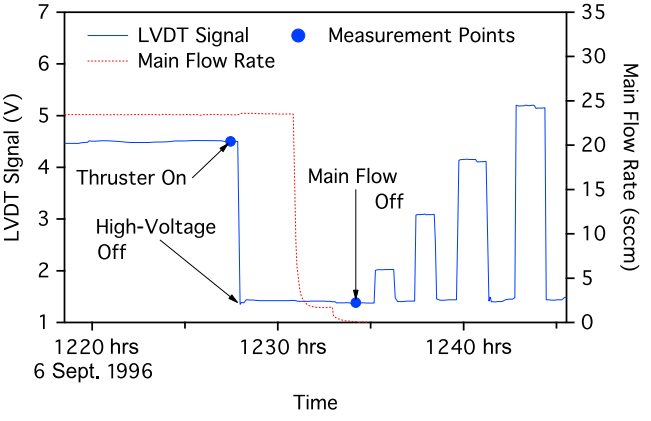

Fig. 18 Example of steady-state thrust measurement [45].

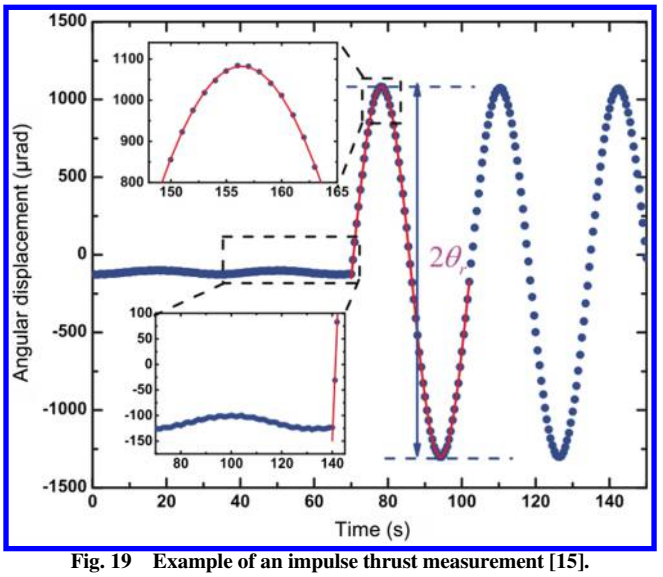

Fig. 19 Example of an impulse thrust measurement [15].

B. Impulse

Data collection for impulse measurements also mirrors the calibration process. After a single impulse, the response data are fitted with a function based on the expected thrust stand dynamics. Figure 19 shows an example of data obtained from a single firing of a pulsed plasma thruster with a torsional pendulum thrust stand. In this case, the data after the pulse have been fitted with a damped sinusoid to estimate the amplitude in the first period. The inset shows a low-amplitude oscillation due to environmental vibrations before the impulse. This can be fit with a separate damped sinusoid, or a range of data before and after the impulse can be fitted with a model that includes noise terms, as discussed previously [Eq. (29)]. The fits yield initial velocity or amplitude data that are converted to impulse bit values using the calibration data. Calibration before and after impulse measurements is also recommended to monitor drift in the thrust stand response.

VI. Errors and Uncertainty Analysis

A. Sources of Error

Instrument errors can be divided into two classes. Random errors are unavoidable at some level and typically are the aggregate result of many small effects, so they tend to follow a normal distribution with a mean of zero. Systematic errors tend to bias the response in a certain direction, so averaging over multiple samples yields a nonzero mean for the error. Different control strategies are employed for random and systematic errors. The uncertainty in the mean value due to random errors may be made arbitrarily small in principle by taking more samples of the measured quantity. Unlike random errors, a systematic bias may be characterized experimentally and subtracted from the measurement to produce a corrected result closer to the true value.

Sources of random error in a pendulum thrust stand response include natural variability in the mechanical response (stiffness of various elements, for example); electrical noise pickup, which may be much worse during thruster operation; transmission of vibrations from the environment to the thrust stand; and vibration due to actuators such as valves on the thrust stand. Additional random errors may enter through the data analysis process, such as errors in the measurement of the distances from the pivot at which thruster and calibration loads are applied. Sources of systematic error include thermal drift, friction between moving and stationary thrust stand components, electromagnetic or electrostatic forces due to high currents or voltages, nonuniform response (amplification or attenuation of higher-frequency thrust components, for example) facility effects such as gas currents, dimensional changes in components due to temperature changes, and drift due to changes in the stiffness of cabling or plumbing.

The calibration process also contributes to the total uncertainty. Random variation in the response to known, fixed loads generally represents a major part of the total uncertainty. Calibration in an environment that differs from that during thruster operation can also lead to random errors or bias. For example, the thermal environment, background pressure, gas flow currents, pressure in propellant lines, and current or voltage in electrical lines may be different or absent during calibration. If these are important parameters, they must be reproduced during calibration or characterized separately so that calibration or measurement data can be corrected. Additional sources of error depend on the particular calibration method. For example, the use of weights and a pulley, as described in Sec. IV, involves uncertainties in the masses of the weights and the fiber or chain, pulley friction, and potential angular offsets in the fiber from the thrust axis.

B. Controlling Systematic Errors

The rate of thrust measurement drift due to thermal effects can be minimized with sufficient cooling along the thermal path between the thruster and the stand, as well as through the use of materials with low thermal conductivity. Placing the stand within an actively cooled shroud will block convective and radiative heat loads to the stand. An effective electrical cable routing design can prevent cable expansion and contraction from pushing or pulling on the stand. Additionally, aligning the connection of electrical cables from the base of the stand to the moving assembly orthogonal to the direction of thrust prevents undesired variable forces on the stand. Active leveling control will eliminate changes in the canting of a thrust stand resulting from thermal fluctuations. Where possible, measuring electrical current in control electronics rather than voltage is advisable in order to avoid errors due to varying voltage drops across cabling caused by temperature fluctuations. Using thermocouples in several locations on the thrust stand can aid in tracking thermal drift effects. As thermal drift is generally unavoidable, frequent stand recalibration is recommended.

Errors caused by friction in the system can be reduced through the use of linear and torsional springs in the thrust stand design. Ensuring that all moving parts are clear of electrical cables and other stationary objects through their entire range of motion is necessary to eliminate intermittent or variable friction and interference. In systems with active damping, free motion of the thrust stand can be verified by turning off the damping system. If there is no parasitic drag due to mechanical interference between moving and stationary parts, the amplitude of the thrust stand oscillations will exhibit a very slow decay. Rapid decay after an impulsive input is an indication of parasitic drag. Attention to cleanliness can prevent unwanted debris from obstructing the motion of the stand. Frequent calibration will also minimize error resulting from gradual changes in friction.

Standard vibrational isolation between the thrust stand base and the vacuum facility can be employed to minimize measurement error due to external sources of vibration. Vibrations can also be actively damped using a force actuator driven by a PID controller. Attaching physical stops that restrict the range of motion of the stand will prevent unexpected vibration or impulses from pushing the stand out of range and possibly damaging components.

Where possible, the use of nonferrous materials in the thrust stand design can help mitigate measurement error due to undesired electromagnetic forces. Maximizing the distance between any magnetic field sources and affected thrust stand components will further reduce measurement errors. Using coaxial or twisted-pair cabling will also reduce interference. If the interaction is unavoidable, characterizing the magnetic tare across the range of possible settings can allow the error to be corrected during data reduction [25,29].

C. Estimating Uncertainties in the Measurement

Despite the best efforts to minimize random errors and eliminate bias, measurement values will always have some uncertainty that represents the range within which the true value is likely to fall. Thrust and impulse measurements should always be reported with an estimate of the uncertainty. The uncertainty analysis involves several steps:

1) Specify equations used to calculate thrust or impulse. The equations used in the data analysis should be written explicitly to identify the components subject to error. These are typically like Eqs. (21 and 28) that relate thrust or impulse to a transducer output with certain calibration measurements.

2) Identify sources of error. Each part of the calibration, data collection, and data analysis processes should be examined to identify potential sources of systematic or random error. The list in Sec. VI.A can serve as a guide, but each individual implementation will be subject to unique sources of uncertainty.

3) Correct for or quantify systematic errors. The first tactic to employ with systematic bias is to determine the physical cause and attempt to eliminate it. Otherwise, the bias should be characterized if possible and a correction applied to the thrust measurement. The uncertainty associated with the correction must be included in the overall uncertainty estimate. If the bias cannot be quantified due to sparse data, the uncorrected measurements should be reported with the probable presence of bias noted and an uncertainty estimate based on the maximum observed bias should be included in the overall uncertainty.

4) Develop an error budget. The uncertainty associated with each potential error source should be estimated and tabulated to assess the validity of analysis methods and quantify errors in the components of the thrust or impulse calculation. The error budget for a calibration process that employs linear model fits (as illustrated previously) is used primarily to verify that the requirements of the linear least-squares analysis are satisfied. The error budget should verify that the uncertainty in the applied calibration loads is much less than the variability of the thrust stand response. If both the dependent and independent variables have significant uncertainty, a conventional least-squares analysis should not be used to estimate model parameters. Alternative methods that properly account for uncertainties in both variables are available [46]. An analysis of the linear fits should demonstrate that the linear model is correct and that disturbances are randomly and uniformly distributed.

The uncertainty of each error source should be characterized by either the standard deviation of multiple measurements or a confidence interval based on the standard deviation. The instrument uncertainty for NIST-traceable standards, such as mass balances or force transducers, may also be used to quantify errors. If statistical methods cannot be used to estimate variability in a component, reasonable physical bounds or engineering judgment can be employed, although these methods are discouraged. For components based on model fit parameters, the uncertainty should be based on the estimate of the variance for the dependent variable. For example, the thrust stand sensitivity is determined from the slope of the calibration line and has a standard deviation

$$s_{S\text{cal}} = \frac{s_x}{\sqrt{\sum_{i=1}^{n} (F_i - \bar{F})^2}} \tag{30}$$

where $\bar{F}$ is the average of the forces used in the calibration. The uncertainty in this parameter is reduced by increasing the number of measurements n, ensuring that the calibration measurements spans the range of expected thrust or impulse values and distributing the calibration points uniformly across the range.

5) Aggregate component errors to determine thrust error. The total uncertainty in the thrust measurement depends on the uncertainties of the individual components in the calculation. If the errors are independent, standard error propagation techniques can be used to determine the aggregate effect on calculated thrust or impulse [47]. For example, the uncertainty in thrust F_t calculated using Eq. (21) is

$$\frac{\sigma_{F_t}}{F_t} = \left[\left(\frac{\sigma_x}{x}\right)^2 + \left(\frac{\sigma_{S\text{cal}}}{S_{\text{cal}}}\right)^2 + \left(\frac{\sigma_{Lt}}{L_t}\right)^2 + \left(\frac{\sigma_{L\text{cal}}}{L_{\text{cal}}}\right)^2 \right]^{1/2} \tag{31}$$

where σ_x can be approximated by s_x [Eq. (25)], $\sigma_{S\text{cal}} \simeq s_{S\text{cal}}$, and σ_{L_t} and $\sigma_{L_{\text{cal}}}$ represent variability in the measurements of L_t and L_{cal}.

In some cases, the thrust or impulse can be interpolated directly from a linear calibration curve. For example, if $L_{cal} = L_t$, the thrust or impulse can be inferred from the plot of response versus calibration loads. The uncertainty in interpolating a value of the independent parameter (F_t, for example) from a measurement of the dependent variable x_t is given by [48,49]

$$s_{F_t} = \frac{s_x}{S_{\text{cal}}} \left[\frac{1}{N} + \frac{1}{n} + \frac{(\bar{x}_t - \bar{x})^2}{S_{\text{cal}}^2 \sum_{i=1}^{n} (F_i - \bar{F})^2} \right]^{1/2} \tag{32}$$

where n is the number of calibration points, N is the number of repeat measurements performed at that operating condition, $\bar{x}_t$ is the mean of the N repeat measurements of the thrust stand response, $\bar{x}$ is the mean of the n responses to the calibration loads F_i, and $\bar{F}$ is the mean of the n calibration values. This equation accounts for uncertainties in the thrust measurements as well as in the calibration curve. It highlights the value of repeat measurements in reducing uncertainty and the fact that higher sensitivity reduces error.

6) Control drift. Unfortunately, pendulum thrust stands are particularly prone to drift due, for instance, to thermal effects. Periodic calibrations or measurements with check standards can be used to control for changes in precision (susceptibility to random errors) and long-term stability (systematic biases).

VII. Recommendations for Reporting Thrust Measurements

Reported thrust measurements should include quantitative estimates of the uncertainty and sufficient information on the measurement method to allow a reader to assess the reliability of the data. We recommend the following guidelines for publications.

1) A brief description of the thrust stand, including the type of displacement sensor, damping mechanisms, and spring components, should be included.

2) A description of the calibration procedure, including the method of applying known forces or impulses, the frequency of calibrations, how the thrust stand zero position is measured or inferred, the number of calibration points n, and the number of repetitions N at each point should be included. A representative plot of calibration data showing the fit and standardized residuals (like those shown in Figs. 11 and 16) and typical values of the square of the correlation coefficient obtained in calibrations should also be included.

3) A quantitative measure of the repeatability of the thrust stand response (the standard deviation of multiple measurements, for instance) for given forces or impulses should be included. The long-term stability of the thrust stand and how drift was controlled or corrected in measurements should also be discussed.

4) The resolution of the thrust stand and how it was determined should be included. If the frequency-dependent thrust noise spectrum is important for the application, a plot of the noise floor similar to Fig. 5 should be included.

5) The thrust stand response time and how it was measured, if the objectives of the study include time-resolved thrust characterization, should be included.

6) A description of the measurement and data analysis methods such as the number of repetitions at a given operation point, how the thrust stand zero was determined, and curve fits employed in impulse measurements should be included.

7) A list of random and systematic error sources, a quantitative assessment of how much each contributes to the total error and how these values were measured or estimated, and a discussion of how systematic errors were controlled or corrected should be included. The total uncertainty should be listed in any tables that include thrust measurements and shown as error bars or confidence intervals on plots of thrust.

VIII. Conclusions

Pendulum thrust stands can provide very accurate measurements of steady-state thrust, time-resolved thrust profiles, and impulse measurements when used properly. Hanging pendulum stands are generally the easiest to implement, but they tend to be less sensitive and often require a large volume. With highly sensitive displacement measurement techniques and control of environmental vibrations and

thermal drift, they can produce high-resolution measurements however. Inverted pendulum stands are typically smaller and more sensitive, and they have been employed with great success to measure millinewton-level thrust in higher-power thrusters. Torsional balances appear to be the most appropriate configuration for microthruster measurements (micronewton-level thrust) and impulse measurements (micronewton-per-second-level impulse bits). The dimensions of the pendulum, the mass of the thruster and mounting hardware, the stiffness of spring components, the damping characteristics of the damping components, and the sensitivity of the displacement transducer are the design parameters that determine the dynamics of the stand and the measurement sensitivity.

The calibration of thrust stands with known forces or impulses is a key part of high-fidelity thrust or impulse measurement. A number of force actuators are available that can be very accurately calibrated and used to impart calibration loads to stands. The design of the calibration procedure has a large influence on the uncertainty in the resulting measurement. Calibration and measurement approaches that determine the thrust stand zero (no-load position) and motion (which reflects the influence of environmental noise) for each measurement are the least susceptible to errors caused by drift.

Thrust measurements should always be corrected for known biases and reported with an estimate of the uncertainty based on a statistical analysis of the data. The error estimate involves documentation of the data analysis process, identification and characterization of potential error sources, estimates of the contributions of each error component, and careful aggregation of component errors into an estimate of the uncertainty in the calculated thrust or impulse. Careful design of the thrust balance and calibration procedure, and a thorough examination of potential sources of error based on experience reviewed in this paper should result in very accurate, reliable thrust data.

Acknowledgments

The research described in this paper was carried out in part by the Jet Propulsion Laboratory, California Institute of Technology, under a contract with NASA. Reference herein to any specific commercial product, process, or service by trade name, trademark, manufacturer, or otherwise does not constitute or imply its endorsement by the U.S. Government or the Jet Propulsion Laboratory, California Institute of Technology.

References

[1] Angeles, J., "Time Response of First- and Second-Order Dynamical Systems," *Dynamic Response of Linear Mechanical Systems: Modeling, Analysis and Simulation*, Springer, New York, 2012, Chap. 2.

[2] Koizumi, H., Komurasaki, K., and Arakawa, Y., "Development of Thrust Stand for Low Impulse Measurement from Microthrusters," *Review of Scientific Instruments*, Vol. 75, No. 10, 2004, pp. 3185–3190. doi:10.1063/1.1790568

[3] McFall, K., and Tilley, D., "Low Power Arcjet Performance Evaluation," *24th International Electric Propulsion Conference*, Electric Rocket Propulsion Soc. Paper IEPC 95-18, Moscow, 1995, http://erps.spacegrant.org/index.php?page=iepc-download-88-07.

[4] Lake, J., Cavallaro, G., Spanjers, G., Adkison, P., and Dulligan, M., "Resonant Operation of a Micro-Newton Thrust Stand," U.S. Air Force Research Lab., Space and Missile Propulsion Division, TR AFRL-PR-ED-TP-2002-308, Edwards AFB, CA, 2003.

[5] Nicolini, D., Frigot, P., Musso, F., Cesare, S., Castorina, G., Ceruti, L., Bartola, F., Zanella, P., Ceccanti, F., Priami, L., and Paita, L., "Direct Thrust and Thrust Noise Measurements on the LISA Pathfinder Field Emission Thruster IEPC-2009-183," *31st International Electric Propulsion Conference*, AIAA Paper 2009-0183, 2009.

[6] Hruby, V., et al., "ST7-DRS Colloid Thruster System Development and Performance Summary," *44th Joint Propulsion Conference*, AIAA Paper 2008-4824, 2008.

[7] Haag, T., "Thrust Stand for Pulsed Plasma Thrusters," *Review of Scientific Instruments*, Vol. 68, No. 5, 1997, pp. 2060–2067. doi:10.1063/1.1148097

[8] Ziemer, J., "Performance Measurements Using a Sub-Micronewton Resolution Thrust Stand," *27th International Electric Propulsion Conference*, AIAA Paper 2001-0238, 2001.

[9] Jamison, A., Ketsdever, A., and Muntz, E., "Gas Dynamic Calibration of a Nano-Newton Thrust Stand," *Review of Scientific Instruments*, Vol. 73, No. 10, 2002, pp. 3629–3637. doi:10.1063/1.1505096

[10] Tew, J., Driessche, J. V. D., Lutfy, F., Muntz, E., Wong, J., and Ketsdever, A., "A Thrust Stand Designed for Performance Measurements of the Free Molecule Micro-Resistojet," *36th Joint Propulsion Conference*, AIAA Paper 2000-3673, 2000.

[11] Rocca, S., Menon, C., and Nicollini, D., "FEEP Micro-Thrust Balance Characterization and Testing," *Measurement Science and Technology*, Vol. 17, No. 4, 2006, pp. 711–718. doi:10.1088/0957-0233/17/4/016

[12] Cubbin, E., Ziemer, J., Choueiri, E., and Jahn, R., "Pulsed Thrust Measurements Using Laser Interferometry," *Review of Scientific Instruments*, Vol. 68, No. 6, 1997, pp. 2339–2346. doi:10.1063/1.1148116

[13] Cesare, S., Musso, F., D'Angelo, F., Castorina, G., Bisi, M., Cordiale, P., Canuto, E., Nicolini, D., Balaguer, E., and Frigot, P.-E., "Nanobalance: The European Balance for Micro-Propulsion," *31st International Electric Propulsion Conference*, AIAA Paper 2009-0182, 2009.

[14] Gamero-Castaño, M., and Hruby, V., "A Torsional Balance for the Characterization of MicroNewton Thrusters," *Review of Scientific Instruments*, Vol. 74, No. 10, 2003, pp. 4509–4514. doi:10.1063/1.1611614

[15] Yang, Y., Tu, L., Yang, S., and Luo, J., "A Torsion Balance for Impulse and Thrust Measurements of Micro-Newton Thrusters," *Review of Scientific Instruments*, Vol. 83, No. 3, Jan. 2012, Paper 015105.

[16] Flores, J., Ingle, M., Robinson, N., and Choudhuri, A., "Development of a Torsional Thrust Balance for the Performance Evaluation of 100mN-5N Thrusters," *47th Joint Propulsion Conference*, AIAA Paper 2011-6016, 2011.

[17] He, Z., Wu, J., Zhang, D., Lu, G., Liu, Z., and Zhang, R., "Precision Electromagnetic Calibration Technique for Micro-Newton Thrust Stands," *Review of Scientific Instruments*, Vol. 84, No. 5, 2013, Paper 055107.

[18] Fowles, G., *Introduction to Modern Optics*, 2nd ed., Dover, Mineola, NY, 1989, Sec. 3.3.

[19] Moeller, T., and Polzin, K., "Thrust Stand for Vertically Oriented Electric Propulsion Performance Evaluation," *Review of Scientific Instruments*, Vol. 81, No. 11, 2010, Paper 115108. doi:10.1063/1.3502463

[20] Polzin, K., Markusic, T., Stanojev, B., DeHoyos, A., and Spaun, B., "Thrust Stand for Electric Propulsion Performance Evaluation," *Review of Scientific Instruments*, Vol. 77, No. 10, 2006, Paper 105108. doi:10.1063/1.2357315

[21] Ketsdever, A., D'Souza, B., and Lee, R., "Thrust Stand Micromass Balance for the Direct Measurement of Specific Impulse," *Journal of Propulsion and Power*, Vol. 24, No. 6, 2008, pp. 1376–1381. doi:10.2514/1.36921

[22] Zafran, S., and Kemp, R., "Colloid Microthruster Test Stand," *AIAA 3rd Flight Test, Simulation, and Support Conference*, AIAA Paper 1969-0314, 1969.

[23] Lilly, T., Ketsdever, A., Pancotti, A., and Young, M., "Development of a Specific Impulse Balance for Capillary Discharge Pulsed Plasma Thrusters," *Journal of Propulsion and Power*, Vol. 25, No. 3, 2009, pp. 823–826. doi:10.2514/1.40261

[24] Pancotti, A., Gilpin, M., and Hilario, M., "Comparison of Electrostatic Fins with Piezoelectric Impact Hammer Techniques to Extend Impulse Calibration Range of a Torsional Thrust Stand," *Review of Scientific Instruments*, Vol. 83, No. 3, 2012, Paper 025109.

[25] Haag, T., "Thrust Stand for High Power Electric Propulsion Devices," *Review of Scientific Instruments*, Vol. 62, No. 5, 1991, pp. 1186–1191. doi:10.1063/1.1141998

[26] Xu, K., and Walker, M., "High-Power, Null-Type, Inverted Pendulum Thrust Stand," *Review of Scientific Instruments*, Vol. 80, No. 5, 2009, Paper 055103.

[27] Nagao, N., Yokota, S., Komurasaki, K., and Arakawa, Y., "Development of a Dual Pendulum Thrust Stand for Hall Thrusters," *43rd Joint Propulsion Conference*, AIAA Paper 2007-5298, 2007.

[28] Boccaletto, L., and d'Agostino, L., "Design and Testing of a Micro-Newton Thrust Stand for FEEP," *36th Joint Propulsion Conference*, AIAA Paper 2000-3268, 2000.

[29] Kodys, A., Murray, R., Cassady, L., and Choueiri, E., "An Inverted-Pendulum Thrust Stand for High-Power Electric Thrusters," *42nd Joint Propulsion Conference*, AIAA Paper 2006-4821, 2006.

[30] Manzella, D., Oleson, S., Sankovic, J., Haag, T., Semenkin, A., and Kim, V., "Evaluation of Low Power Hall Thruster Propulsion," *32nd Joint Propulsion Conference*, AIAA Paper 1996-2736, 1996.

[31] Tartler, B., "Construction and Performance of an Inverted Pendulum Thrust Balance," M.S. Thesis, Massachusetts Inst. of Technology, Cambridge, MA, 2010, Secs. 3.2–3.5.

[32] Manzella, D., and Jankovsky, R., "Laboratory Model 50 kW Hall Thruster," *38th Joint Propulsion Conference*, AIAA Paper 2002-3676, 2002.
[33] Garner, C., Brophy, J., Polk, J., and Pless, L., "Cyclic Endurance Test of a SPT-100 Stationary Plasma Thruster," *30th Joint Propulsion Conference*, AIAA Paper 1994-2856, 1994.
[34] Shabshelowitz, A., Gallimore, A., and Peterson, P., "Performance of a Helicon Hall Thruster Operating with Xenon, Argon, and Nitrogen," *Journal of Propulsion and Power*, Vol. 30, No. 3, 2014, pp. 664–671. doi:10.2514/1.B35041
[35] Pote, B., and Hruby, V., "Performance of a Multi-Kilowatt Non-Circular Discharge Hall Thruster," *36th Joint Propulsion Conference*, AIAA Paper 2000-3249, 2000.
[36] Patterson, M., Haag, T. W., and Rawlin, V. K., "NASA 30 cm Ion Thruster Development Status," *30th Joint Propulsion Conference*, AIAA Paper 1994-2849, 1994.
[37] Soulas, G., Haag, T., Herman, D., Huang, W., Kamhawi, H., and Shastry, R., "Performance Test Results of the NASA-457M v2 Hall Thruster," *49th Joint Propulsion Conference*, AIAA Paper 2012-3940, 2012.
[38] Markusic, T., Jones, J., and Cox, M., "Thrust Stand for Electric Propulsion Performance Evaluation," *40th Joint Propulsion Conference*, AIAA Paper 2004-3441, 2004.
[39] Chatterjee, S., and Price, B., *Regression Analysis by Example*, Wiley, New York, 1977, Secs. 1.6–1.7.
[40] Anscombe, F. J., "Graphs in Statistical Analysis," *American Statistician*, Vol. 27, No. 1, 1973, pp. 17–21.
[41] Wilson, M., Bushman, S., and Burton, R., "A Compact Thrust Stand for Pulsed Plasma Thrusters," *25th International Electric Propulsion Conference*, Electric Rocket Propulsion Soc. Paper IEPC 97-122, Cleveland, OH, 1997, http://erps.spacegrant.org/index.php?page=iepc-download-88-07.
[42] Selden, N., and Ketsdever, A., "Comparison of Force Balance Calibration Techniques for the Nano-Newton Range," *Review of Scientific Instruments*, Vol. 74, No. 12, 2003, pp. 5249–5254. doi:10.1063/1.1623628
[43] Johnson, W., and Warne, L., "Electrophysics of Micromechanical Comb Actuators," *Journal of Microelectromechanical Systems*, Vol. 4, No. 1, 1995, pp. 49–59. doi:10.1109/84.365370
[44] Ziemer, J., Cubbin, E., Choueiri, E., and Birx, D., "Performance Characterization of a High Efficiency Gas-Fed Pulsed Plasma Thruster," *33rd Joint Propulsion Conference*, AIAA Paper 2004-2925, 1997.
[45] Polk, J., Anderson, J., Brophy, J., Rawlin, V., Patterson, M., and Sovey, J., "The Results of an 8200 Hour Wear Test of the NSTAR Ion Thruster," *35th Joint Propulsion Conference*, AIAA Paper 1999-2446, 1999.
[46] Fuller, W., " A Single Explanatory Variable," *Measurement Error Models*, Wiley, New York, 1987, Chap. 1.
[47] Taylor, J., *An Introduction to Error Analysis*, University Science Books, Mill Valley, CA, 1982, Sec. 8.4.
[48] Salter, C., "Error Analysis Using the Variance-Covariance Matrix," *Journal of Chemical Education*, Vol. 77, No. 9, 2000, pp. 1239–1243. doi:10.1021/ed077p1239
[49] Prichard, L., and Barwick, V., "Preparation of Calibration Curves: A Guide to Best Practice," LGC Group, Ltd. TR LGC/VAM/2003/032, Teddington, Middlesex, U.K., 2003.

J. Blandino
Associate Editor